Artificial neural network-based multiple-input multiple-output metamodel for prediction of design parameters for a high-speed rail viaduct

Susmita Panda, Arnab Banerjee, Ajinkya Baxy, Bappaditya Manna & Sondipon Adhikari

Taylor & Francis
Taylor & Francis Group

Check for updates

Artificial neural network-based multiple-input multiple-output metamodel for prediction of design parameters for a high-speed rail viaduct

Susmita Panda[a], Arnab Banerjee[a], Ajinkya Baxy[b], Bappaditya Manna[a] and Sondipon Adhikari[c]

[a]Department of Civil Engineering, Indian Institute of Technology Delhi, Hauz Khas, India; [b]Department of Mechanical Engineering, Visvesvaraya National Institute of Technology, Nagpur, India; [c]James Watt School of Engineering, The University of Glasgow, Glasgow, UK

ABSTRACT

The prediction of the design parameters of short to medium-span supported bridges in critical locations (such as canal/road crossings) under the action of high-speed trains has been investigated in this article. An artificial neural network (ANN)-based MIMO (multiple-input multiple-output) metamodels is proposed in conjunction with the semi-analytical framework of simply-supported bridges. Three cases, namely single moving load, series of moving loads at equal spacing (HSLM-B), and as per conventional train configuration (HSLM-A) recommended in Eurocode1: EN 1991-2 (2003), are considered. The prime novelty of the article is to develop a dimensionless semi-analytical framework to train and validate a MIMO metamodel implementing ANN for predicting the multiple dynamic responses of bridges under high-speed loads. The dependency of the maximum dynamic responses, that is, displacement, shear force, and bending moment, on the governing parameters (structural and loading) have been elucidated using Pearson's correlation matrix for the three different train configurations. Further, the robustness and efficiency of the best-fitted metamodels have been compared, and a user interface has been developed for ease of implementation. This platform evaluates the responses such as displacement, shear force, bending moment, and structural safety confirming the standards of Eurocode EN 1990:2002 + A1:2005 (E).

1. Introduction

The emergence of a high-speed guided transit system is the most pivotal alternative for transportation planning (Sugawara, 1995). The important attributes of high-speed rail (HSR) such as speed, reliability, safety, and comfort have made comprehending travellers choose rail as their effective means of communication (Li & Schmöcker, 2017). However, the structural safety and stability of the high-speed rail bridges are questionable due to their increased speed (Cantero et al., 2016; Garmendia et al., 2012; Jin & Feng, 2020). The problem is aggravated especially in the case of the simply-supported bridges as their displacement response is more than that of a continuous bridge. More than 70% of the bridges in developed countries are simply-supported (Kang et al., 2018), particularly in situations such as canal/road crossing. Additionally, due to ease in construction and cost-effectiveness, multi-pier flyovers and elevated bridges have evolved from simply supported segmental modules. This topic has sought the attention of many engineers and researchers to develop strategies towards understanding the systematic mechanism of transmission of dynamic moving load on the supporting structures (Arvidsson & Karoumi, 2014; Gbadeyan & Oni, 1995; Grandi & Ramondenc, 1990; Kaynia et al., 2000; Olsson, 1991; Xia & Zhang, 2005; Yau et al., 1999). However, such analyses are computationally very expensive.

To deal with this, a predictive metamodel employing artificial neural networks (ANN) is developed in this article to conserve computational effort and reduce the amount of expertise needed in the preliminary evaluation of dynamic responses. Metamodels, also known as response surfaces, black-box models, surrogate models, or emulators, are useful tools to mimic complex systems' input/output behaviour with relaxed accuracy in a given domain (Han et al., 2012; Kullaa, 2009; Wang et al., 2014). ANN-based surrogate models were widely used for predictive maintenance or damage detection of bridges (Goldberg, 2013; Modarres et al., 2018; Suryanita & Adnan, 2013, 2014; Wedel & Marx, 2022). The list of various surrogate modelling techniques in the state-of-art articles presented in Gordan et al. (2022), Sun et al. (2020), and Yu et al. (2016) include multivariate adaptive regressive spline models, random forests, single hidden-layer feed-forward ANNs, radial basis function network, support vector machines, Gaussian process regression, automated learning of algebraic models, etc. A comparative analysis of different predictive methods has been presented for evaluating bridge response: multilinear regression, artificial neural network, and regression tree (Mete et al., 2019). An improved response surface method (RSM) and linear adaptive weighted RSM (LAW-RSM) for assessing the reliability of the time-dependent non-linear behaviour of high-speed railway bridges were developed by Cho et al. (2010).

Various uncertainties, including stiffness, a moment of inertia, damping of the primary suspension of the vehicle, and

geometrical and mechanical properties of girders and slabs were considered. Based on non-linear autoregressive with exogenous input (NARX), a surrogate model was developed to analyse the vehicle–bridge systems subjected to stochastic excitation (Han et al., 2019; Li et al., 2021b; Rocha et al., 2016). Such a method forecasts dynamic responses better than two-time numerical simulation (or Monte Carlo simulation). Further, by using a feed-forward neural network and deep long short-term memory network, the prediction of time and frequency response of vehicle–bridge interaction were conducted in (Li et al., 2021a). The effect of track irregularities and noise level on predicting dynamic responses was also investigated. With the aid of Bayesian regularised back propagation neural network, the dynamic responses of long-span bridges under the random effects of winds and waves were investigated in (Fang et al., 2020; Salcher et al., 2019). Such a method effectively captures the non-linear vibration characteristic response of the bridge under larger wind and wave loads. To date, the dedicated research using ANN in the available literature (Mete et al., 2019; Ok et al., 2012; Xu, 2020) focussed only on training problems of MISO (multiple-input single-output) types and the literature addressing problems of MIMO (multiple-input multiple-output) types is quite scarce (Li et al., 2022; Tang et al., 2022).

This article proposes a semi-analytical methodological framework for efficient prediction of bridge responses, including displacement, shear force, and bending moment, using analytical modelling. Further, to bypass the extensive computation, an ANN-based MIMO metamodel is developed in this article. Based on the developed mathematical formulation for moving load over the bridge, non-dimensional input and output parameters are derived to produce data for the training of neural networks. The concept of non-dimensionalization optimises the entire computation process and increases efficiency. The robustness of the proposed metamodel is verified with the actual analytical model. Moreover, the prediction ability of the present framework is investigated by developing a user interface to allow researchers and engineers to design simply-supported bridges with various ranges of parameters. A user-friendly platform for comparing the resulting response with the codal provision has also been made within the interface.

2. Mathematical formulation

In this section, a semi-analytical framework is formulated for the problem idealising the elevated bridge subjected to moving loads travelling at speed v over the length of bridge L at time t as shown in Figure 1. The bridge is simplified as a simply-supported Euler-Bernoulli beam with vertical vibration modes under different dynamic moving load cases to represent the behaviour of moving train loads. Figure 1(c) shows the modelling of the moving load as a single load. However, the series of load as illustrated in Figure 1d,e can be modelled as high-speed load models (HSLM) mentioned in Eurocode (Bsi, 2002), i.e. HSLM-B and HSLM-A. The HSLM-B model consists of a series of loads separated at equal axle spacing of d as shown in Figure 1d. Similarly, a conventional train model in which each bogie consists of a four-wheel assembly can be simplified into HSLM-A as shown in Figure 1e.

To retain the deterministic nature of the semi-analytical framework, the vehicle-track interaction (track and rail irregularities) has been ignored. However, by suitably including the structural damping ratio, the effects of train-bridge interaction can be established (Museros & Alarcón, 2002). Further, the inclusion of rail irregularities has not been considered as it can be a stochastic process that may not be a topic of concern for the present scenario. The elastic and inertial effects of the vehicle have been ignored by considering the smaller ratio of the vehicle to bridge mass. Therefore, the train models are kept general as moving forces as suggested by Eurocode1: EN 1991-2 (2003).

2.1. Equation of motion of beam under the effect of dynamic moving loads

The governing equation of motion of the beam (with damping) under the action of a moving vehicle can be given as follows (Yang et al., 1997):

$$\rho A \frac{\partial^2 \widetilde{W_b}(x,t)}{\partial t^2} + EI \frac{\partial^4 \widetilde{W_b}(x,t)}{\partial x^4} + C_b \frac{\partial \widetilde{W_b}(x,t)}{\partial t} = P_V, \quad (1)$$

where ρA, EI, C_b and P_V = mass per unit area, flexural rigidity, damping coefficient of the bridge, forces due to the moving load; $\tilde{W}_b$ = dynamic displacement of the bridge at position x and time t and $\delta(x)$ represents Dirac delta function. The forcing function for different load models can be defined as follows:

- For single load model as shown in Figure 1b:

$$P_V = \delta(x - vt)P_1 P(t), \quad (2)$$

where P_1 and $P(t) = \left[H(t) - H\left(t - \frac{L}{v}\right)\right]$ are the gravitational weight of the running train and step function, respectively.

- As per Eurocode model "HSLM-B" as shown in Figure 1c

$$P_V = \sum_{n=1}^{N} P_N \delta[x - v(t - t_k)]P(t), \quad (3)$$

where $t_k = (k-1)\frac{d}{v}$ is the time taken by the kth load with corresponding step function $P(t) = [H(t - t_k) - H(t - \frac{L}{v} - t_k)]$.

- As per Eurocode model 'HSLM-A' as shown in Figure 1d

$$\begin{aligned} P_V = &\sum_{n=1}^{N} P_1 \delta[x - v(t - t_{kD})]P(t_1) \\ &+ \sum_{n=1}^{N} P_2 \delta\left[x - v\left(t - \frac{b}{v} - t_{kD}\right)\right]P(t_2) \\ &+ \sum_{n=1}^{N} P_3 \delta\left[x - v\left(t - \frac{b+c}{v} - t_{kD}\right)\right]P(t_3) \\ &+ \sum_{n=1}^{N} P_4 \delta\left[x - v\left(t - \frac{2b+c}{v} - t_{kD}\right)\right]P(t_4), \end{aligned} \quad (4)$$

where $t_{kD} = (k-1)\frac{D}{v}$ is the time delay of the kth bogie with corresponding step function as follows:
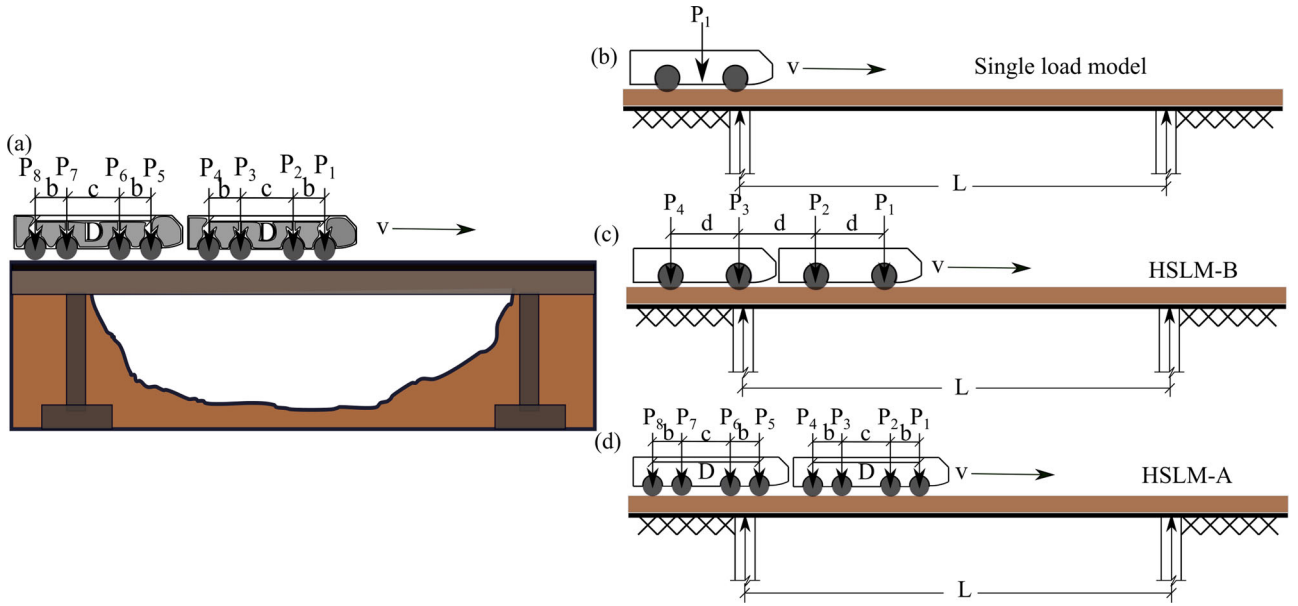
Figure 1. (a) Conceptualisation of model of elevated simply-supported bridge unit under the action of moving loads; (b) simplified idealisation of moving load as single load model; (c) simplified idealisation of series of moving load spaced at equidistant to each other (HSLM-B train model); and (d) simplified idealisation of series of loads as per conventional train model (HSLM-A train model).
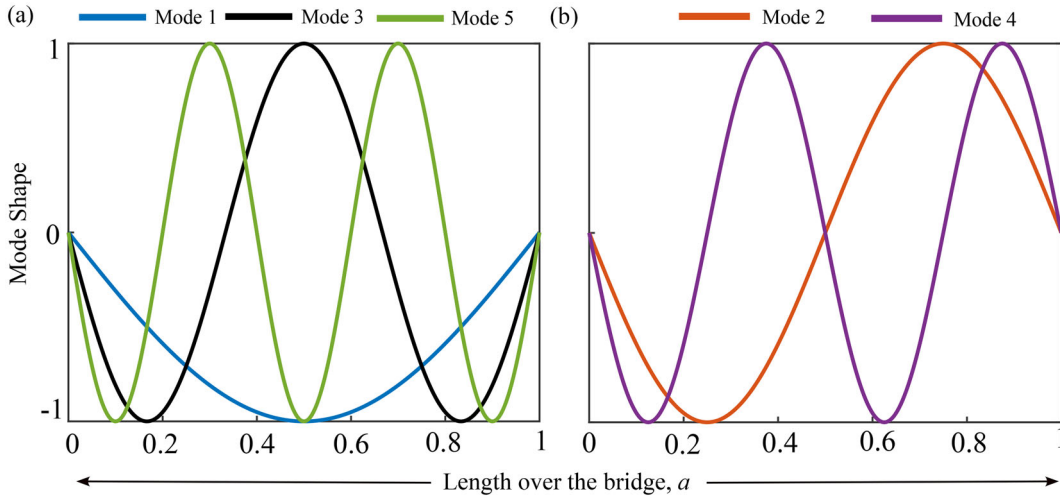
Figure 2. Mode-shape of a simply-supported beam for (a) odd modes; (b) even modes.

$$P(t_1) = \left[H(t - t_{kD}) - H\left(t - \frac{L}{v} - t_{kD} \right) \right],$$

$$P(t_2) = \left[H\left(t - \frac{b}{v} - t_{kD} \right) - H\left(t - \frac{L}{v} - \frac{d}{v} - t_{kD} \right) \right],$$

$$P(t_3) = \left[H\left(t - \frac{b+c}{v} - t_{kD} \right) - H\left(t - \frac{L}{v} - \frac{b+c}{v} - t_{kD} \right) \right],$$

$$P(t_4) = \left[H\left(t - \frac{2b+c}{v} - t_{kD} \right) - H\left(t - \frac{L}{v} - \frac{2b+c}{v} - t_{kD} \right) \right],$$

$$(5)$$

2.2. Modal superposition method

Using the modal superposition method, the order of governing equation of motion presented in Equation (1) can be reduced.

In this method, the dynamic displacement $\tilde{W}_b(x,t)$ can be assumed as a function of generalised coordinate $\tilde{Q}_{bj}(t)$ and shape function $\phi_j(x)$. The mode shapes of a simply-supported beam are of sinusoidal nature as evidenced in Figure 2. Thus, the dynamic displacement $\tilde{W}_b(x,t)$ can be expressed as follows:

$$\widetilde{W}_b(x,t) = \sum_{j=1}^{\infty} \tilde{Q}_{bj}(t)\phi_j(x) \approx \sum_{j=1}^{J} \tilde{Q}_{bj}(t) \sin\left(\frac{j\pi x}{L} \right). \quad (6)$$

Correspondingly, shear force $\tilde{V}$ and bending moment $\tilde{M}$ can be given as follows:

$$\tilde{V} = EI \frac{d^3 \widetilde{W}_b}{dx^3} = EI \frac{d^3}{dx^3} \left(\sum_{j=1}^{J} \tilde{Q}_{bj}(t)\phi_j(x) \right)$$

$$= EI \frac{d^3}{dx^3} \left(\sum_{j=1}^{N} \tilde{Q}_{bj}(t) \sin \frac{j\pi x}{L} \right),$$

$$(7)$$

$$\tilde{M} = -EI\frac{d^2\widetilde{W_b}}{dx^2} = -EI\frac{d^2}{dx^2}\left(\sum_{j=1}^{N}\tilde{Q}_{bj}(t)\phi_j(x)\right)$$

$$= -EI\frac{d^2}{dx^2}\left(\sum_{j=1}^{J}\tilde{Q}_{bj}(t)\sin\frac{j\pi x}{L}\right). \quad (8)$$

Using the above mode superposition method, Equation (1) becomes

$$\rho A\sum_{j=1}^{N}\ddot{\tilde{Q}}_{bj}(t)\phi_j(x) + C_b\sum_{j=1}^{N}\dot{\tilde{Q}}_{bj}(t)\phi_j(x)$$

$$+ EI\frac{j^4\pi^4}{L^4}\sum_{j=1}^{N}\tilde{Q}_{bj}(t)\phi_j(x) = P_V. \quad (9)$$

Multiplying $\phi_i(x)$ to both sides of Equation (9) and integrating from 0 to L, we get

$$\ddot{\tilde{Q}}_{bj}(t)\sum_{j=1}^{N}\int_0^L\phi_i(x)\phi_j(x)dx + \frac{C_b}{\rho A}\dot{\tilde{Q}}_{bj}(t)\sum_{j=1}^{N}\int_0^L\phi_i(x)\phi_j(x)dx$$

$$+\frac{EI}{\rho A}\frac{j^4\pi^4}{L^4}\tilde{Q}_{bj}(t)\sum_{j=1}^{N}\int_0^L\phi_i(x)\phi_j(x)dx = \frac{1}{\rho A}\int_0^L\phi_i(x)(P_V)dx. \quad (10)$$

Using orthogonality principle of mode shapes, replacing subscript ϕ_i into ϕ_j, Equation (10) reduces to

$$\ddot{\tilde{Q}}_{bj} + 2\zeta_b\omega_{bj}\dot{\tilde{Q}}_{bj} + \omega_{bj}^2\tilde{Q}_{bj} = \frac{\int_0^L\phi_j(x)(P_V)dx}{\rho A\int_0^L\phi_j^2(x)dx}, \quad (11)$$

where ω_{bj} is the natural frequency of the beam given as follows:

$$\omega_{bj}^2 = \frac{j^4\pi^4}{L^4}\left(\frac{EI}{\rho A}\right), \quad (12)$$

and ζ_b is the damping coefficient expressed as the ratio of the damping constant to the critical damping constant ($C_c = 2\rho A\omega_{bj}$).

Some of the influential non-dimensional parameters have been introduced as follows: The dimensionless displacement of beam $\widetilde{Q}_{bj}(x,t)$ can be given as follows:

$$\frac{\tilde{Q}_{bj}(x,t)}{\Delta_{st}} = Q_{bj}(a,\tau), \quad (13)$$

where Δ_{st} is an arbitrary constant called static displacement.

The dimensionless length and time can be represented as follows:

$$a = x/L, \quad \tau = \omega_b t, \quad (14)$$

where t is the total time taken by the moving load under velocity v to traverse through the length of the beam L.

A speed parameter η can be introduced to define the ratio of the frequency of load ω to the natural frequency of the beam ω_b as follows:

$$\eta = \frac{\omega}{\omega_b} = \frac{\pi v}{L}\frac{L^2}{\pi^2}\sqrt{\frac{\rho A}{EI}}. \quad (15)$$

2.2.1. Case-1: Single moving load

The numerator of Equation (11) i.e. the forcing function due to vehicle P_V can be solved as follows:

$$\int_0^L P_V\phi_j dx = \int_0^L\delta(x-vt)P_oP(t)\phi_j(x)dx$$

$$= P_oP(t)\phi_j(vt) = P_oP(t)\sin\left(\frac{j\pi vt}{L}\right). \quad (16)$$

From η, the velocity v can be written as follows:

$$v = \frac{L\omega_b\eta}{\pi}. \quad (17)$$

Using Equation (14) and Equation (17), the inner term of Equation (16) can be modified as (for single moving load):

$$\int_0^L P_V\phi_j dx = P_oP(t)\sin(j\eta\tau). \quad (18)$$

Similarly for moving load at equidistant, inner term Equation (16) can be written as follows:

$$\int_0^L P_V\phi_j dx = P_oP(t)\sin\left(j\frac{\pi v}{L}(t-t_k)\right)$$

$$= P_oP(t)\sin\left[j\frac{\pi L\omega_b\eta}{\pi L}\left(\frac{\tau}{\omega_b}-\frac{\bar{\tau}}{\omega_b}\right)\right]$$

$$= P_oP(t)\sin[j\eta(\tau-\bar{\tau})]. \quad (19)$$

Using Equations (13) and (14) of non-dimensional parameters, Equation (11) becomes

$$\omega_b^2\ddot{Q}_{bj} + 2\zeta_b\omega_{bj}\omega_b\dot{Q}_{bj} + \omega_{bj}^2 Q_{bj} = \frac{2}{L\rho A}\left[\left(\frac{P_oP(t)}{\Delta_{st}}\right)\sin j\eta\tau\right]. \quad (20)$$

Dividing the Equation (20) by ω_b^2, we get

$$\ddot{Q}_{bj} + 2\zeta_b\frac{\omega_{bj}}{\omega_b}\dot{Q}_{bj} + \frac{\omega_{bj}^2}{\omega_b^2}Q_{bj} = \frac{2}{L\rho A\omega_b^2}\left[\left(\frac{P_oP(t)}{\Delta_{st}}\right)\sin j\eta\tau\right]. \quad (21)$$

The value of $\frac{\omega_{bj}}{\omega_b} = j^2$ can be substituted in Equation (21)

$$\ddot{Q}_{bj} + 2j^2\zeta_b\dot{Q}_{bj} + j^4 Q_{bj} = \left[\left(\frac{2P_o}{\omega_b^2 L\rho A\Delta_{st}}\right)P(t)\sin j\eta\tau\right]. \quad (22)$$

Let

$$\frac{2P_o}{L\rho A\Delta_{st}\omega_b^2} = 1 \quad (23)$$

or using Equation (12), Δ_{st} can be written as follows:

$$\Delta_{st} = \frac{2P_oL^4\rho A}{L\rho A\pi^4 EI} = \frac{2P_oL^3}{\pi^4 EI}. \quad (24)$$

Equation (21) for single moving load can be re-written using Equation (15) parameters as follows:

$$\ddot{Q}_{bj} + 2j^2\zeta_b\dot{Q}_{bj} + j^4 Q_{bj} = P(t)\sin j\eta\tau. \quad (25)$$

The generalised coordinate Q_{bj} for forced vibration during $\Delta t \leq t_{i+1} \leq \Delta t + \frac{L}{V}$, i.e. the force is on the bridge can be given as (Yang et al., 1997):

$$Q_{bj} = \frac{1}{(1-\eta^2)^2 + (2\zeta_b\eta)^2}\left[(1-\eta^2)\sin(j\eta\tau) - 2\zeta_b\eta\cos(j\eta\tau)\right],$$

(26)

where t_{i+1} is the time step of the next iteration. When the force has left the bridge, $t_{i+1} \geq \Delta t + \frac{L}{V}$, the free vibration response induced can be written as:

$$Q_{bj} = \frac{1}{(1-\eta^2)^2 + (2\zeta_b\eta)^2}$$
$$\left(\eta e^{(-\tau\zeta_b)}\left[2\zeta_b\cos\tau\sqrt{(1-\zeta_b^2)} - \frac{(1-\eta^2-2\zeta_b^2)}{\sqrt{(1-\zeta_b^2)}}\sin\tau\sqrt{(1-\zeta_b^2)}\right]\right).$$

(27)

The total response of the beam (forced + free) can be rewritten as:

$$Q_{bj} = \frac{1}{(1-\eta^2)^2 + (2\zeta_b\eta)^2}\left(\left[(1-\eta^2)\sin(j\eta\tau) - 2\zeta_b\eta\cos(j\eta\tau)\right]\right.$$
$$+ \eta e^{(-\tau\zeta_b)}\left[2\zeta_b\cos\tau\sqrt{(1-\zeta_b^2)} - \frac{(1-\eta^2-2\zeta_b^2)}{\sqrt{(1-\zeta_b^2)}}\right.$$
$$\left.\left.\sin\tau\sqrt{(1-\zeta_b^2)}\right]\right).$$

(28)

Equation (28) can be written in reduced form as follows:

$$Q_{bj} = F\left[(1-\eta^2)\sin(a_1) - 2\zeta_b\eta\cos(a_1)\right.$$
$$\left. + \eta e^{(-\tau\zeta_b)}(2\zeta_b\cos(b_1) - G\sin(b_1)\right],$$

(29)

where $F = \frac{1}{(1-\eta^2)^2+(2\zeta_b\eta)^2}$, $a_1 = j\eta\tau$, $b_1 = \tau\sqrt{(1-\zeta_b^2)}$ and $G = \frac{(1-\eta^2-2\zeta_b^2)}{\sqrt{(1-\zeta_b^2)}}$. Thus, the total displacement of the beam in summation form can be written as follows:

$$W_b(a,\tau) = \sum_{j=1}^{\infty} F\left[(1-\eta^2)\sin(a_1) - 2\zeta_b\eta\cos(a_1)\right.$$
$$\left. + \eta e^{-(\tau\zeta_b)}(2\zeta_b\cos(b_1) - G\sin(b_1)\right]\sin j\pi a.$$

(30)

Accordingly, the shear force $\tilde{V}$ given in Equation (7) for the beam under the action of moving loads can be computed as follows:

$$\tilde{V} = \frac{EI}{L^3}\left(\sum_{j=1}^{N}Q_{bj}(\tau)\Delta_{st}\frac{d^3}{da^3}\sin(j\pi a)\right)$$
$$= j^3\pi^3\frac{EI}{L^3}\Delta_{st}\left(\sum_{j=1}^{N}Q_{bj}(\tau)\cos(j\pi a)\right).$$

(31)

The shear force in dimensionless form, V, can be written as follows:

$$V = \frac{\tilde{V}L^3}{EI\pi^3\Delta_{st}} = j^3\left(\sum_{j=1}^{N}Q_{bj}(\tau)\cos(j\pi a)\right),$$

(32)

$$= j^3\sum_{j=1}^{\infty}F\left[(1-\eta^2)\sin(a_1) - 2\zeta_b\eta\cos(a_1)\right.$$
$$\left. + \eta e^{(-\tau\zeta_b)}(2\zeta_b\cos(b_1) - G\sin(b_1)\right]\cos(j\pi a).$$

(33)

Similarly, the bending moment $\tilde{M}$ in Equation 8 can be written as

$$\tilde{M} = -\frac{EI}{L^2}\left(\sum_{j=1}^{N}Q_{bj}(\tau)\Delta_{st}\frac{d^2}{da^2}\sin j\pi a\right)$$
$$= -j^2\pi^2\frac{EI}{L^2}\Delta_{st}\left(\sum_{j=1}^{N}Q_{bj}(\tau)\sin j\pi a\right).$$

(34)

The corresponding bending moment in dimensionless form can be written as

$$M = \frac{\tilde{M}L^2}{EI\pi^2\Delta_{st}} = -j^2\left(\sum_{j=1}^{N}Q_{bj}(\tau)\sin j\pi a\right)$$
$$= -j^2\sum_{j=1}^{\infty}F\left[(1-\eta^2)\sin(a_1) - 2\zeta_b\eta\cos(a_1)\right.$$
$$\left. + \eta e^{(-\tau\zeta_b)}(2\zeta_b\cos(b_1) - G\sin(b_1)\right]\sin j\pi a.$$

(35)

2.2.2. Case-2: Loads spaced at equidistant - HSLM-B

For HSLM-B model, Equation (21) can be written as follows:

$$\ddot{Q}_{bj} + 2\zeta_b j^2\dot{Q}_{bj} + j^4 Q_{bj} = \sum_{K=1}^{N}P(t)\sin(j\eta(\tau - \bar{\tau})),$$

(36)

where $t_k = \frac{\pi\epsilon(k-1)}{\eta}$ is the dimensionless time taken by the kth load, $\epsilon = \frac{d}{L}$ is the dimensionless distance between the adjacent loads. and $\bar{\tau} = \omega_b t_k$ is the time delay of the k_{th} load on the bridge. Using the concept of a single load model on a beam, the generalised solution for HSLM-B can be obtained as follows:

$$Q_{bj} = F\left[AH(\tau - \bar{\tau}) + (-1)^{n+1}BH\left(\tau - \frac{\pi}{\eta} - \bar{\tau}\right)\right],$$

(37)

where the coefficients of Equation (37) can be simplified as

$$A = \sin(c_1) - 2\zeta_b\eta\cos(c_1)$$
$$+ \eta e^{(-\tau\zeta_b)}[2\zeta_b\cos(d_1) - G\sin(d_1)],$$

(38)

$$B = \sin(c_2) - 2\zeta_b\eta\cos(c_2)$$
$$+ \eta e^{(-\tau\zeta_b)}[2\zeta_b\cos(d_2) - G\sin(d_2)],$$

(39)

where $c_1 = j\eta(\tau - \bar{\tau})$, $d_1 = \sqrt{(1-\zeta_b^2)}(\tau - \bar{\tau})$, $c_2 = j\eta\left(\tau - \frac{\pi}{\eta} - \bar{\tau}\right)$ and $d_2 = \sqrt{(1-\zeta_b^2)}\left(\tau - \frac{\pi}{\eta} - \bar{\tau}\right)$

2.2.3. Loads represented as bogies-HSLM-a

For HSLM-A model, Equation (21) can be written as follows:

$$\ddot{Q}_{bj} + 2\zeta_b j^2 \dot{Q}_{bj} + j^4 Q_{bj} = \sum_{K=1}^{N} P(t) \big[\sin\left(j\eta(\tau - \bar{\tau}_D)\right)$$
$$+ \sin\left(j\eta(\tau - \bar{\tau}_b - \bar{\tau}_D)\right) \quad (40)$$
$$+ \sin\left(j\eta(\tau - \bar{\tau}_c - \bar{\tau}_D)\right)$$
$$+ \sin\left(j\eta(\tau - \bar{\tau}_e - \bar{\tau}_D)\right)\big],$$

where $t_{kD} = \frac{\pi\epsilon_D(k-1)}{\eta}$ is the time taken by k^{th} bogie separated by $\epsilon_D = \frac{D}{L}$ as shown in Figure 1e,f with corresponding time lag $\bar{\tau}_D = \omega_b t_{kD}$. Similarly $t_b = \frac{\epsilon_b \pi}{\omega_b \eta}$ is the time taken distance between loads P_{t1} and P_{t2} separated by $\epsilon_b = \left(\frac{b}{L}\right)$ with time lag $\bar{\tau}_b = \omega_b t_b$, $t_c = \frac{\epsilon_c \pi}{\omega_b \eta}$ is the time taken between loads P_{t1} and P_{t3} separated by distance $\epsilon_c = \left(\frac{b+c}{L}\right)$ with time lag $\bar{\tau}_c = \omega_b t_c$, $t_e = \frac{\epsilon_e \pi}{\omega_b \eta}$ is the time taken between loads P_{t1} and P_{t4} separated by $\epsilon_e = \left(\frac{2b+c}{L}\right)$ and time lag $\bar{\tau}_e = \omega_b t_e$ respectively.

Adopting the similar procedure as followed for the HSLM-B model, the generalised coordinate for HSLM-A can be given as follows:

$$Q_{bj} = F\Big[A_1 H(\tau - \bar{\tau}_D) + A_2(-1)^{j+1} H\left(\tau - \frac{\pi}{\eta} - \bar{\tau}_D\right)$$
$$+ B_1 H(\tau - \bar{\tau}_b - \bar{\tau}_D) + B_2(-1)^{j+1} H\left(\tau - \bar{\tau}_b - \frac{\pi}{\eta} - \bar{\tau}_D\right)$$
$$+ C_1 H(\tau - \bar{\tau}_c - \bar{\tau}_D) + C_2(-1)^{j+1} H\left(\tau - \bar{\tau}_c - \frac{\pi}{\eta} - \bar{\tau}_D\right)$$
$$+ D_1 H(\tau - \bar{\tau}_e - \bar{\tau}_D) + D_2(-1)^{j+1} H\left(\tau - \bar{\tau}_e - \frac{\pi}{\eta} - \bar{\tau}_D\right)\Big],$$
$$(41)$$

where

$$A_1 = \sin(c_1) - 2\zeta_b \eta \cos(c_1)$$
$$+ \eta e^{(-\tau\zeta_b)}[2\zeta_b \cos(d_1) - G\sin(d_1)], \quad (42)$$
$$A_2 = \sin(c_2) - 2\zeta_b \eta \cos(c_2)$$
$$+ \eta e^{(-\tau\zeta_b)}[2\zeta_b \cos(d_2) - G\sin(d_2)], \quad (43)$$
$$B_1 = \sin(c_3) - 2\zeta_b \eta \cos(c_3)$$
$$+ \eta e^{(-\tau\zeta_b)}[2\zeta_b \cos(d_3) - G\sin(d_3)], \quad (44)$$

Table 2. Various output parameters.

Dimensional output parameter	Factor	Dimensionless output parameter
Displacement, $\widetilde{Q_{bj}}$	$\Delta_{dis} = \frac{2PL^3}{\pi^4 EI}$	$Q_b = \frac{\widetilde{Q_b}}{\Delta_{dis}}$
Shear force, $\widetilde{V_{bj}}$	$\Delta_{sf} = \frac{2P}{\pi}$	$V_b = \frac{\widetilde{V_b}}{\Delta_{sf}}$
Bending moment, $\widetilde{M_b}$	$\Delta_{bm} = \frac{2PL}{\pi^2}$	$M_b = \frac{\widetilde{M_b}}{\Delta_{bm}}$

$$B_2 = \sin(c_4) - 2\zeta_b \eta \cos(c_4)$$
$$+ \eta e^{(-\tau\zeta_b)}[2\zeta_b \cos(d_4) - G\sin(d_4)], \quad (45)$$
$$C_1 = \sin(c_5) - 2\zeta_b \eta \cos(c_5)$$
$$+ \eta e^{(-\tau\zeta_b)}[2\zeta_b \cos(d_5) - G\sin(d_5)] \quad (46)$$
$$C_2 = \sin(c_6) - 2\zeta_b \eta \cos(c_6)$$
$$+ \eta e^{(-\tau\zeta_b)}[2\zeta_b \cos(d_6) - G\sin(d_6)], \quad (47)$$
$$D_1 = \sin(c_7) - 2\zeta_b \eta \cos(c_7)$$
$$+ \eta e^{(-\tau\zeta_b)}[2\zeta_b \cos(d_7) - G\sin(d_7)], \quad (48)$$
$$D_2 = \sin(c_8) - 2\zeta_b \eta \cos(c_8)$$
$$+ \eta e^{(-\tau\zeta_b)}[2\zeta_b \cos(d_8) - G\sin(d_8)], \quad (49)$$

where $c_3 = j\eta(\tau - \bar{\tau}_b)$, $d_3 = \sqrt{(1-\zeta_b^2)}(\tau - \bar{\tau}_b - \bar{\tau}_D)$, $c_4 = j\eta\left(\tau - \bar{\tau}_b - \frac{\pi}{\eta} - \bar{\tau}_D\right)$, $d_4 = \sqrt{(1-\zeta_b^2)}\left(\tau - \bar{\tau}_b - \frac{\pi}{\eta} - \bar{\tau}_D\right)$, $c_5 = j\eta(\tau - \bar{\tau}_c - \bar{\tau}_D)$, $d_5 = \sqrt{(1-\zeta_b^2)}\left(\tau - \bar{\tau}_c - \frac{\pi}{\eta} - \bar{\tau}_D\right)$, $c_6 = j\eta(\tau - \bar{\tau}_c - \bar{\tau}_D)$ and $d_6 = \sqrt{(1-\zeta_b^2)}\left(\tau - \bar{\tau}_c - \frac{\pi}{\eta} - \bar{\tau}_D\right)$, $c_7 = j\eta(\tau - \bar{\tau}_e - \bar{\tau}_D)$ and $d_7 = \sqrt{(1-\zeta_b^2)}\left(\tau - \bar{\tau}_e - \frac{\pi}{\eta} - \bar{\tau}_D\right)$, $c_8 = j\eta(\tau - \bar{\tau}_e - \bar{\tau}_D)$ and $d_8 = \sqrt{(1-\zeta_b^2)}\left(\tau - \bar{\tau}_e - \frac{\pi}{\eta} - \bar{\tau}_D\right)$.

A summary of the dimensionless design parameters for the different models and their corresponding output has been listed in Tables 1 and 2, respectively, which governs the design of simply-supported bridges under the action of

Table 1. Input parameters.

Dimensional input parameters	Dimensionless input parameters
Speed of moving load, v	$\eta = \frac{\pi v}{L\omega_b}$
Flexural rigidity, EI	
Mass per unit length, ρA	
Natural frequency of the beam, ω_b	$\omega_b = \frac{\pi^2}{L^2}\sqrt{\frac{EI}{\rho A}}$
Damping of the beam, ζ	—
Distance between the adjacent loads, L_d	$\epsilon_d = \frac{L_d}{L}$
Distance between the adjacent bogies, L_b	$\epsilon_b = \frac{L_b}{L}$
Distance between the adjacent car units, L_c	$\epsilon_c = \frac{L_c}{L}$
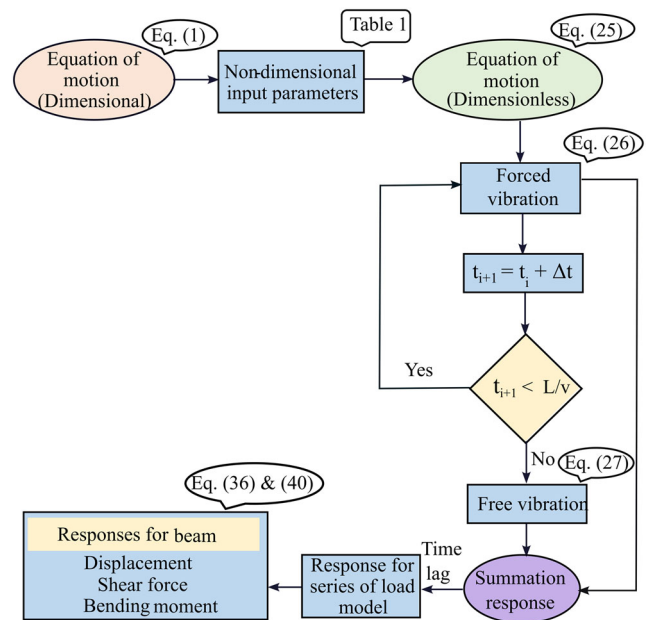
Figure 3. Flowchart of the proposed analytical model.
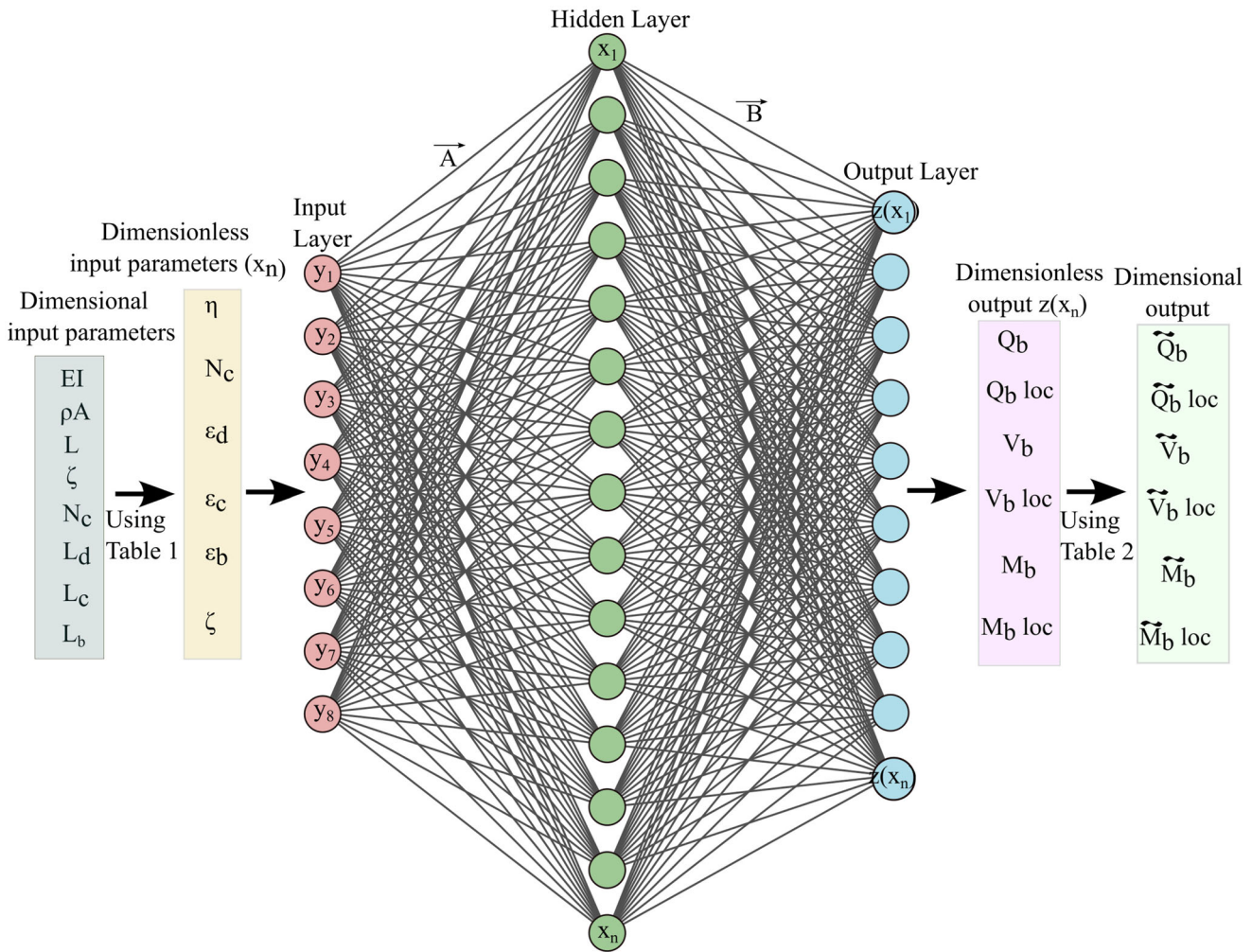
Figure 4. Architecture of ANN network diagram for MIMO model.

Table 3. Computational efficiency.

	Computational time (s)	
Number of time step	Theoretical solution	Metamodels
10	2–3	1–2
100	300–400	2–4
1000	800–1000	5–8

moving loads. Additionally, a flowchart has been shown in Figure 3 to recap the entire analytical procedure.

3. Application of artificial neural network (ANN) in problems considering the moving load analysis over simply-supported beams

The application of ANN-based metamodels to predict the dynamic behaviour of various systems is widely reported in the literature (Huang & Fu, 2019; Lu et al., 2012; Salehi & Burgueño, 2018; Thai, 2022; Vodithala et al., 2020). However, implementing the MIMO metamodel with a generalised feed-forward (GFF) neural network is an improvement over traditional MISO problems. The connection between neurons of non-adjacent layers in GFF makes the process trained with supervised learning. A schematic of a typical metamodel ANN architecture is illustrated in Figure 4. ANNs comprise node layers containing an input layer, one or more hidden layers, and an output layer. Each of these layers contains a connection of interconnected neurons. An ANN can learn the complicated relationship between the input and output parameters based on the interconnections of the layers via neurons. As a rule of thumb, the number of hidden neurons should be 2/3 the size of the input layer, plus the size of the output layer, or less than twice the size of the input layer. The number of neurons in the hidden layer to achieve good accuracy depends on how complicated the dataset you are using to train your ANN. Further, the efficiency of a trained dataset is determined if the overfitting of the model has been prevented. In this case, we have used a regularisation technique called early stopping which enables the training to be automatically stopped when a chosen metric has stopped improving. The analysis has been performed with 7 hidden layers and neurons varying from 5 - 300. An ANN can learn the complicated relationship between the input and output parameters based on the interconnections of the layers via neurons and associated weight and threshold. Further, there are no back-loops in the feed-forward network, i.e. nodes never form a cycle. The input data is weighted by weighing vectors $\vec{A}$ and $\vec{B}$, as shown in Figure 3, summed up and,

Table 4. Pearson correlation coefficient (Edwards, 1976).

Pearson's correlation		
Strong	Moderate	Weak
0.7–1.0	0.3–0.7	0–0.3
Positive values	Proportionally correlated	
Negative values	Inversely correlated	

if the neuron is activated, then passed on to the next neuron. The activation function plays a pivotal role in activating a neuron. The usage of sigmoid and hyperbolic tangent activation functions is usually not recommended in networks with multiple hidden layers due to vanishing gradient problems. However, the rectified linear activation function (ReLU) which can be given as $f(a) = \max\{0, a\}$ possesses two major benefits: sparsity (when $a \leq 0$) and a reduced likelihood of vanishing gradient. This feature allows the model to learn faster and perform better and hence has been used as an activation function in the present study. The present analysis has been performed with Intel(R) Xeon(R) E-2186G CPU @ 3.80 GHz, 3792 Mhz having 6 Core(s). Table 3 shows the computational efficiency between theoretical solutions and metamodels. It can be found that metamodels are much faster than conventional theoretical methods for solving the same problem with higher time steps.

3.1. Data generation and training

A flowchart provided in Figure 5 gives an insight into the entire process involved in training and validating the model. In this work, the beam and vehicle parameters (such as length of the beam, material properties and fundamental frequency of the beam, damping of the beam, speed of moving load, number of car units, the distance between adjacent car units, etc.) are used as an input parameter to the metamodel and the network is trained to predict the various parameters such as dynamic displacement, shear force and bending moment. A complete list of the input and output parameters is tabulated in Table 1. The data required to train the ANN was generated using the procedure described in Section 2.2. Note, the procedure discussed in Section 2.2 was verified against the published literature. The data thus generated was categorised into training data (70%) and testing data (30%). Due to various orders present in the input data, it was normalised using the Min-Max scheme. Such a scheme ensures that all the input data lies between zero and one, thus eliminating any bias. The training data was used to train the network to create a model which minimises the mean square error function.

3.2. Metrics for evaluation of the bridge responses

The statistical performance indicators such as the mean square error (MSE), root mean square error (RMS) and explained variance score (EVS) are used in the analysis to assess the reliability of the developed MIMO metamodel. The MSE value determines the mean error between the estimated and measured values. Alternatively, it measures the
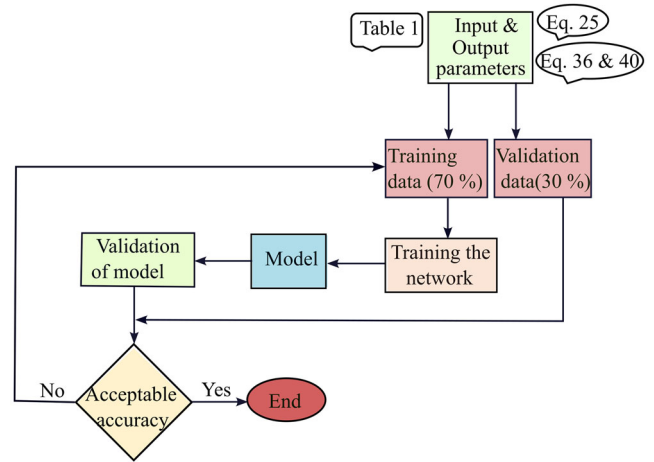
Figure 5. Flowchart for training and validation of the dataset.

Table 5. Bridge and load parameters for single moving load (Yang et al., 2004).

Item	Notation	Value
Length of the bridge	L	20 m
Elastic rigidity	EI	10 Gpa
Mass per unit length	m	3000 kg/m
Damping of the beam	ζ_b	2.50%
Mass of moving load	P	6 kN
Fundamental frequency of bridge	ω_b	14.25 rad/sec
Speed of vehicle	v	27.78 m/s

Table 6. Bridge and load parameters for series of moving load (Yang et al., 2004).

Item	Notation	Value
Length of the bridge	L	20 m
Modulus of elasticity	E	29.43 GPa
Moment of inertia	I	3.81 m^4
Mass per unit length	ρA	34,088 kg/m
Number of bogies	N_b	5
Mass of each bogie	P	22,000 kg
Distance between loads	a	24 m
Speed of vehicle	v	34 m/s

variance of residuals or non-fit in the population. However, RMS is a standardised measure of the degree of fit in the sample or how accurately the network predicts the measured output. The EVS or coefficient of determination explains the dispersion of errors of a given dataset, and quantile-quantile plots are also used to evaluate the network performance. Let us consider the predicted value of the ith sample to be $\bar{z}_i$ and z_i is the corresponding measured (actual) value over n samples, then the metric parameters can be calculated as follows:

$$MSE(z, \bar{z}) = \frac{1}{n} \sum_{i=1}^{n-1} |z_i - \bar{z}_i|, \; EVS(z, \bar{z})$$

$$= 1 - \frac{\sum_{i=1}^{n} (z_i - \bar{z}_i)^2}{\sum_{i=1}^{n} (z_i - z)^2}, \; RMS = \frac{\sum_{i=1}^{n} (\bar{z}_i - z_i)^2}{\sum_{i=1}^{n} ((z) - z_i)^2},$$

$$(50)$$

where $z = \frac{1}{n} \sum_{i=1}^{n} z_i$.

The sensitivity analysis of different output parameters on the input parameters can be measured using the Pearson
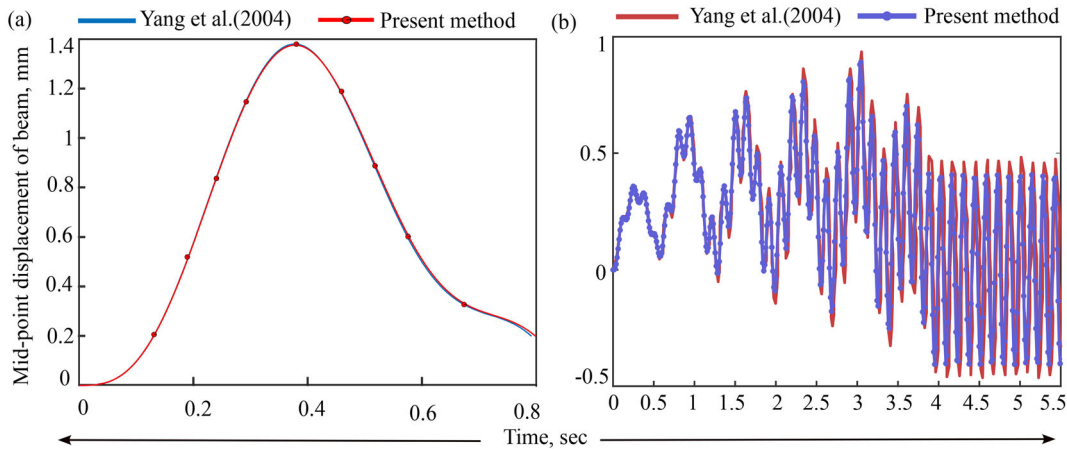
Figure 6. Comparison of the mid-point displacement response of the simply-supported beam for (a) single moving load; (b) Series of load as per HSLM-B model.

correlation coefficient, widely called PCC or the bivariate correlation (Benesty et al., 2009; Edwards, 1976; Glen, 2021; Sedgwick, 2012), or simply as the correlation coefficient which is a measure of linear correlation between two sets of data. It can be defined as the ratio between the covariance of two variables and the product of their standard deviations; which ranges between −1 to 1. The strength of a parameter can be defined as weak, moderate, and strong depending upon the range mentioned in Table 4. The positive values indicate a direct relationship between input and output parameters, i.e. if the input parameter increases, the resultant output also increases. However, the negative values imply the inversely proportional relationship between input and output parameters and vice-versa in the case dictated above.

4. Results and discussion

4.1. Validation of the proposed theory

The effectiveness of the proposed method has been elucidated by considering a simply-supported beam under the effect of a single load moving at a speed of $100 \, \text{km/h} = 27.78$ m/s and a series of load models (HSLM-B) at a resonance speed of 32 m/s. The details regarding the bridge and load parameters are mentioned in Tables 5 and 6 adopted from Yang et al. (2004). The dimensionless displacement obtained at the mid-point of the beam under can be transformed into a dimensional one by multiplying the constant, the so-called static displacement Δ_{st}. It can be observed in Figure 6 that the dynamic mid-point displacement of the beam is consistent with the results published in the literature, which provides confidence in the developed model for further analysis.

A detailed discussion of the results obtained from the analytical solution and MIMO metamodel is described in the following section. The resulting responses of a beam, displacement, shear force, and bending moment, as mentioned in Table 2, have been investigated in detail for different load models.

4.2. Single moving load

Most of the existing studies in the literature are confined to a single mode for the sake of brevity in the analysis.

However, consideration of the higher modes allows us to verify the location of the maximum response, which has extreme significance in designing. In this section, the analysis with higher modes was performed to check the convergence of the total response, which consists of forced and free vibration. Figure 7a and 7a1 shows the variation of dimensionless displacement with respect to the speed parameter, η. The value of η has varied from 0 to 3 in order to consider both the effect of speed as well as to understand the influence of free and forced vibrations. For most of the short-span girders of length shorter than 30 m and speed of traversing being 140 km/h, values of η less than 0.5 are sufficient. However, η greater than 0.5 finds application in most of the bridges with extremely high speeds (Yang et al., 2004). It can be noticed that the higher modes of displacement response converge to the first mode. The total response of the bridge increases rapidly from $\eta = 0.2$, attains a maximum value at $\eta_{max} = 0.6$ or, and decreases after that. The response is predominantly governed by forced vibration and yields maximum dynamic amplification at a lower speed parameter. The maximum displacement occurs at the mid-point of the simply-supported bridge for higher vibration modes, as indicated in Figure 7b because the shape function of the higher even modes ($j = 2, 4, 6, \ldots$) is asymmetrical. Therefore, the range of η from 0.2 to 0.8 is of utmost importance for designing simply-supported high-speed rail bridges.

Some of the specific points of η, i.e. 0.147, 0.199, 0.63, 1, 1.76, 2.28, were chosen to study the total response (displacement) in-depth with the square root of the sum of squares of the first three modes' response. The brighter colour of the contour maps indicates the maximum displacement with time on one axis and space on the other, as shown in Figure 7c–h. For the values of $\eta < 1$ as shown in Figure 7c–f, the maximum amplitude occurs due to the forced vibration and for $\eta > 1$, the free vibration influences the response which lasts longer and then decays with time as shown in Figure 7g,h.

Figure 8 shows maximum shear force and bending moment in dimensionless form and their variation along the bridge length to speed parameter for different modes (1, 3, 5, and 10). Figure 8 (a) and (b) show that the shear force
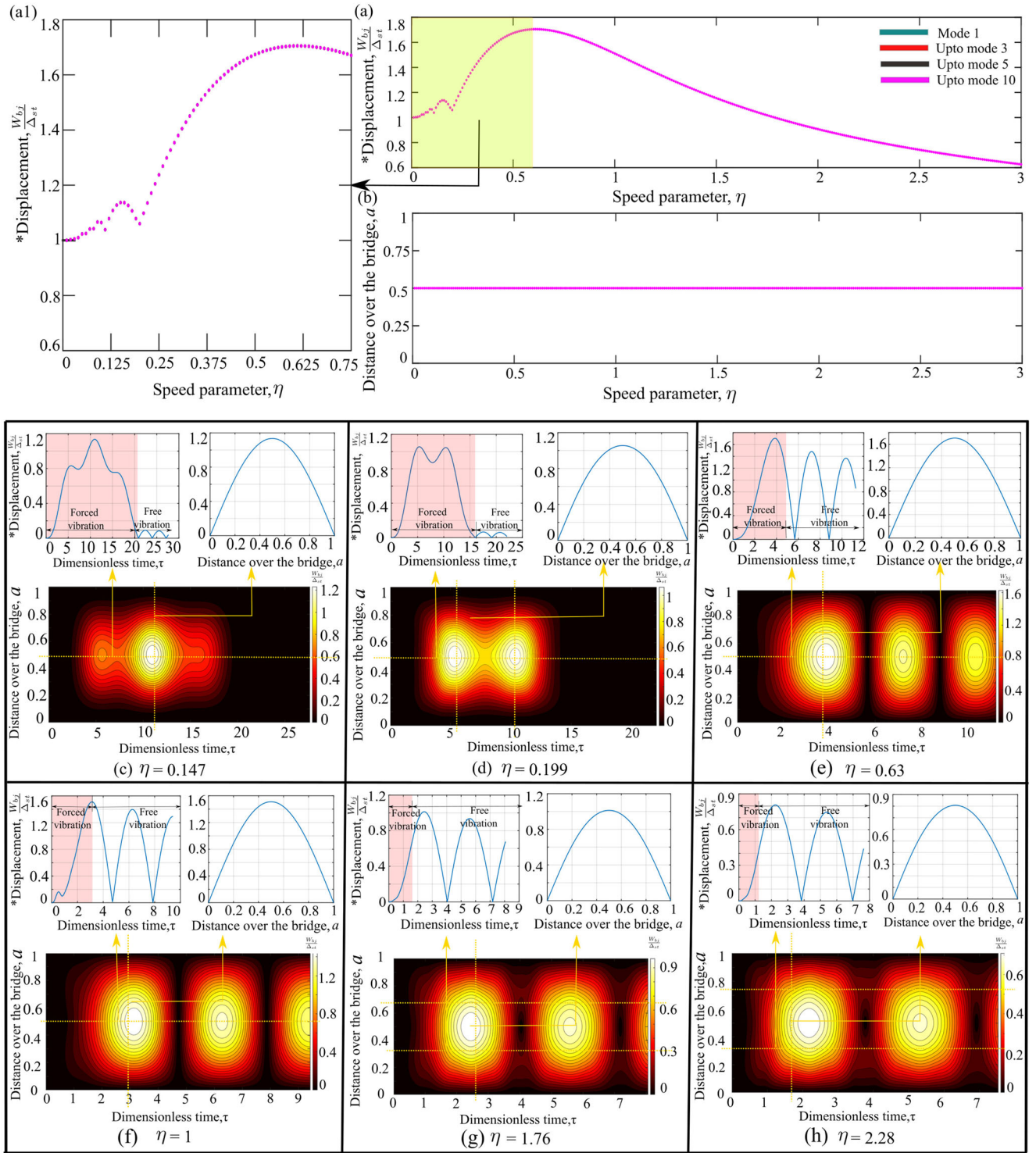
Figure 7. (a)*Dimensionless maximum displacement $\frac{W_{bj}}{\Delta_{st}}$; (a1) enlarged view of Fig.(a) for η upto 0.7; (b) position a over the bridge (a) with respect to the speed parameter η; (c) contour for $\eta = 0.147$; (d) contour for $\eta = 0.199$; (e) contour for $\eta = 0.63$; (f) contour for $\eta = 1$; (g) contour for $\eta = 1.76$; (h) contour for $\eta = 2.28$ with respect to time and length over the bridge a.

response which occurs at one of the support of the simply-supported bridge does not converge and increases for higher modes with increasing η.

However, the higher modes of the bending moment response converge to the first mode for $\eta < 1.5$. While the values of $\eta > 1.5$, the bending moment response converges from third modes as shown in Figure 8e. A similar observation in the location of the bending moment has been

noticed. For values of $\eta < 1.5$, the maximum bending moment occurs at the mid-point whereas for values of $\eta > 1.5$, it bifurcates towards the ends of the beam as shown in Figure 8f. The influence of higher modes, particularly on shear force and bending moment, is due to the presence of the additional term, for instance, j^3 for shear force and j^2 for bending moment as described in Equations (31) and (34). It all depends on the vibration mode that has been
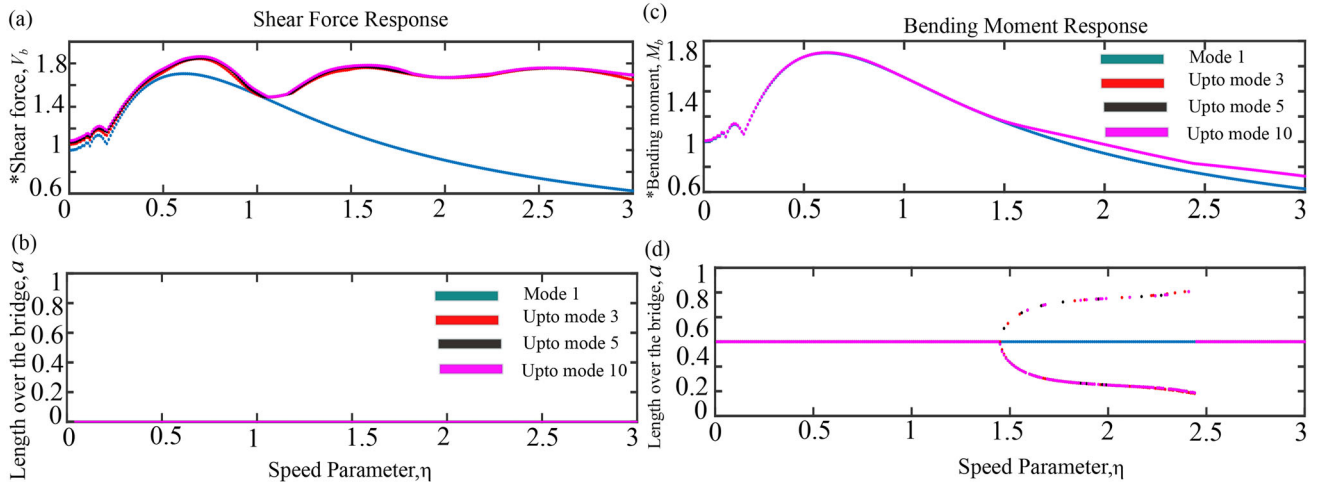
Figure 8. (a) *Dimensionless maximum shear force $\frac{V_b}{\Delta_{st}}$ versus speed parameter η; (b) position of maximum amplitude of $\frac{V_b}{\Delta_{st}}$ over the length of the bridge a versus speed parameter η; (c) *Dimensionless maximum bending moment $\frac{M_b}{\Delta_{st}}$ versus speed parameter η; (d) Position of maximum amplitude of $\frac{M_b}{\Delta_{st}}$ over the length of the bridge a versus speed parameter η.
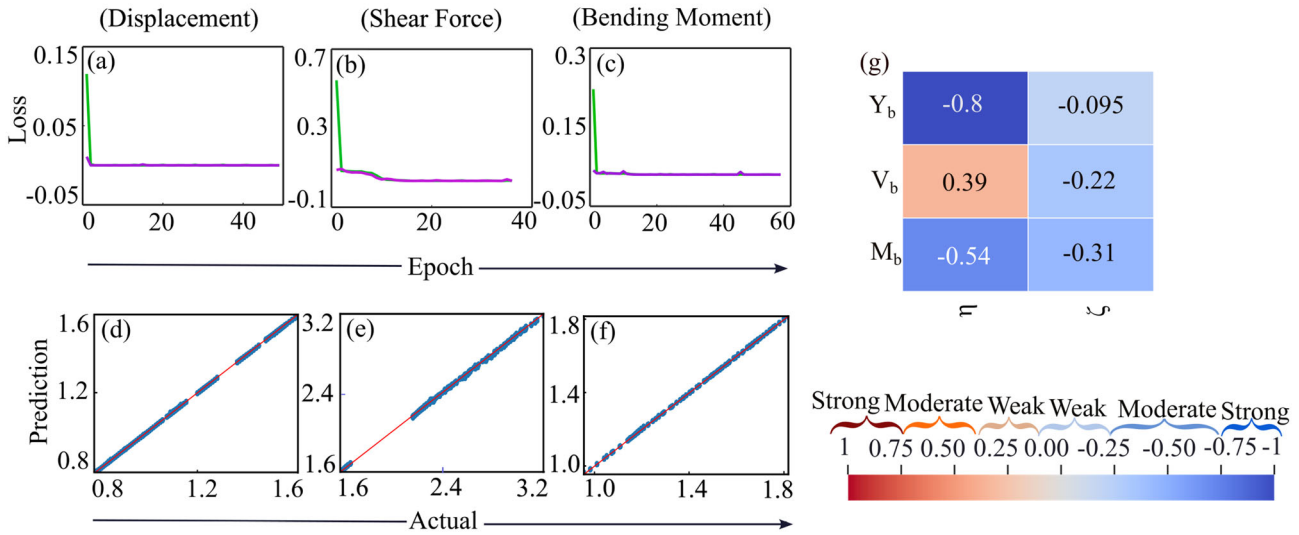
Figure 9. Loss versus epoch for (a) displacement; (b) shear force; (c) Bending moment; Prediction versus actual for (d) displacement; (e) shear force; (f) bending moment; and (g) Pearson correlation matrix with speed parameter η and damping ζ for single load model.

Table 7. Metrices for the single load model.

	Single load model		
Output parameter	MSE	RMS	EVS
Displacement	0.00304	0.0036	0.9999
Shear Force	0.00713	0.0092	0.9995
Bending moment	0.00149	0.0019	0.9999

Table 8. Comparison of analytical and the ML-based model for single load model.

Speed (m/s)	38.32	67.56	96.81	126.06
η	0.42	0.74	1.06	1.39
ζ	0.033	0.022	0.038	0.005
$\bar{Y}_b\,(m)$	0.001571	0.00165	0.00141	0.00127
$\bar{Y}_{b\,ML}\,(m)$	0.001572	0.0017	0.00142	0.00126
Error (%)	0.26	0.36	0.37	0.92
$V_b\,(kN)$	7.78	10.38	8.21	11.19
$\bar{V}_{b\,ML}\,(kN)$	7.75	10.42	8.28	11.11
Error (%)	0.41	0.37	0.93	0.68
$M_b\,(kN.m)$	40.74	42.43	36.24	40.27
$\bar{M}_{b\,ML}\,(kN.m)$	40.61	42.31	35.98	40.12
Error (%)	0.33	0.28	0.68	0.26

excited where the resonant frequency gets interfered with the higher frequency of the beam. Similar observations were also reported by (Yang et al., 2004). Therefore, the computational design of simply-supported bridges should be made with a minimum of the first three modes recommended by (Bsi, 2002).

The loss (training and validation) versus epoch for various output parameters listed in Table 2 are plotted in Figure 9a–c. From these figures, it is evident that the overfitting of the model is avoided. In addition, the quantile-quantile plot of the prediction and actual values are shown in Figure 9d–f. The best-fitted metamodels through ANN are achieved with a value of $R^2=0.99$, and other metrics such as MSE, RMS, and EVS have been listed in Table 7.
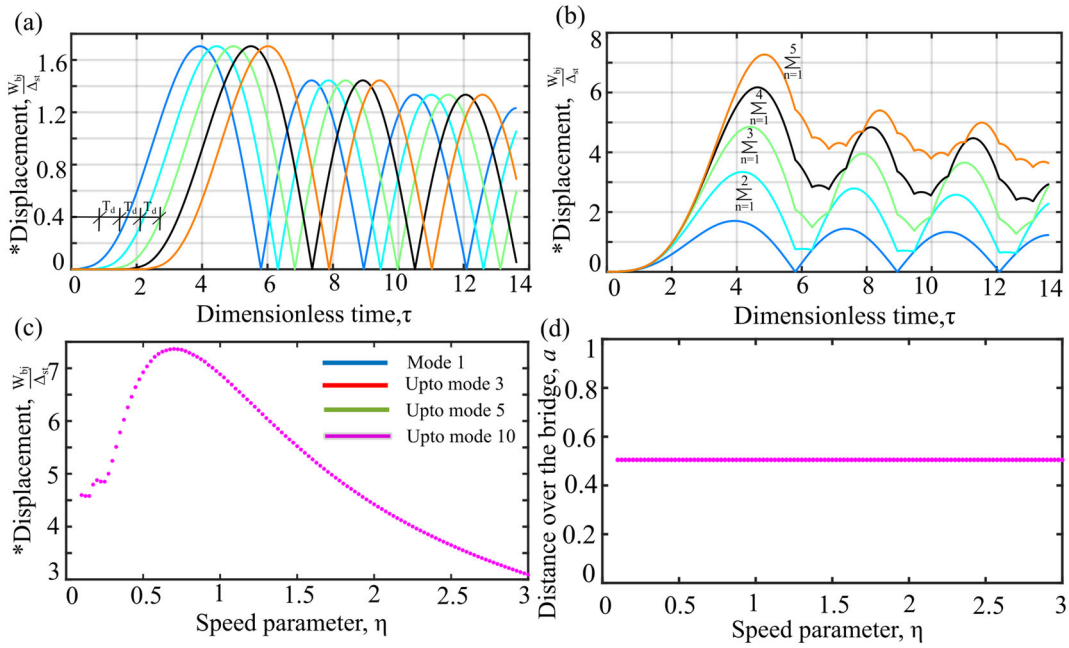
Figure 10. *Dimensionless displacement; (a) series of load (N = 5) with time lag $\epsilon = 0.1$ at $\eta = 0.6$; (b) Cumulative response of series of loads; (c) convergence of different modes; and (d) distance over the bridge a.

The dependency of various output parameters on various input parameters has been thoroughly investigated through sensitivity analysis as shown in Figure 9. A comparison between the analytical solution and ANN-based model is established, and their corresponding error percentages are mentioned in Figure 8.

Based on Pearson's classification as described in Table 4, the input parameters can be correlated as per their strength indicated in Figure 9g. The speed parameter has a moderate negative linear relationship with displacement and a weak negative relationship with bending moment. Referring to Table 8, it can be observed that with an increasing value of η, the amplitude of displacement of the beam decreases. Similar observations were reported for bending moment also. The reason can be attributed to the fact that the displacement increases up to a critical speed (η ranging between 0.6 and 1) and then decreases. A similar observation has been reported in the analytical model as shown in Figure 7. An error of less than 1% is noticed for displacement and bending moment with the fitted models.

However positive relationship of speed parameter exists for shear force, i.e., with an increasing value of η, the shear force in the beam increases as clearly evident in Table 8 and pretty well matches the mathematical results with error percentage less than 1%. The next parameter under observation is the damping of the beam, which plays a crucial role in suppressing most of the vibrational energy–the lower values of damping results in higher amplitude of responses and vice-versa. Thus damping of the beam indicates a weak to moderate influence on the output parameters.

4.3. HSLM

The short-span bridges ($L < 7$ m) can be analysed using HSLM-B as per Eurocode provision (Bsi, 2002) where train

loads are idealised as a series of loads lagging by an equal amount. Figure 10 (a) shows the dimensionless displacement response for series of loads (N-loads $= 5$) situated at equidistant to each other with a time lag T_d. In addition, their combined response has been shown in Figure 10b. The analysis has been conducted for different modes ($j = 1$, 3, 5, 10), and it can be observed in Figure 10c,d that the higher modes of the displacement response occur at the mid-point of the simply-supported bridge converges to the first mode.

The variation of maximum displacement has been shown in Figure 11a–d using contour maps for governing parameters, i.e. speed parameter, η and the ratio of the distance between loads to the length of the bridge ϵ for the number of loads ($N = 5$, 10, 15, 20). The possible combinations of the distance between the wheelset to the length of the bridge (ϵ) have been analysed to assess the best-fit range of values that can minimise the amplification of responses due to moving loads. The dynamic displacement for the different number of loads for values of $\epsilon = 0.1$, 0.6, and 0.8 has been presented in Figure 11. It can be noticed that the dynamic displacement for values of $\epsilon = 0.6$ and 0.8 is much lower as compared to $\epsilon = 0.1$. Further, it can be confirmed from contours that if the distance between loads, i.e. ($\epsilon = 0.1$), is small, the displacement values are quite large. This states that if the loads are closer, their responses can interfere with each other and lead to excessive deformation of the bridge deck. However, their interference can be minimised if they are at an optimal distance apart.

Figure 12a shows the variation of maximum responses of the bridge in dimensionless form normalised concerning the highest value of the response that occurred for 20 loads. The values with which normalisation has been performed are 21.58 for displacement, 23.93 for shear force, and 21.58 for bending moment, respectively. It can be observed that responses increase with the increasing number of loads. The
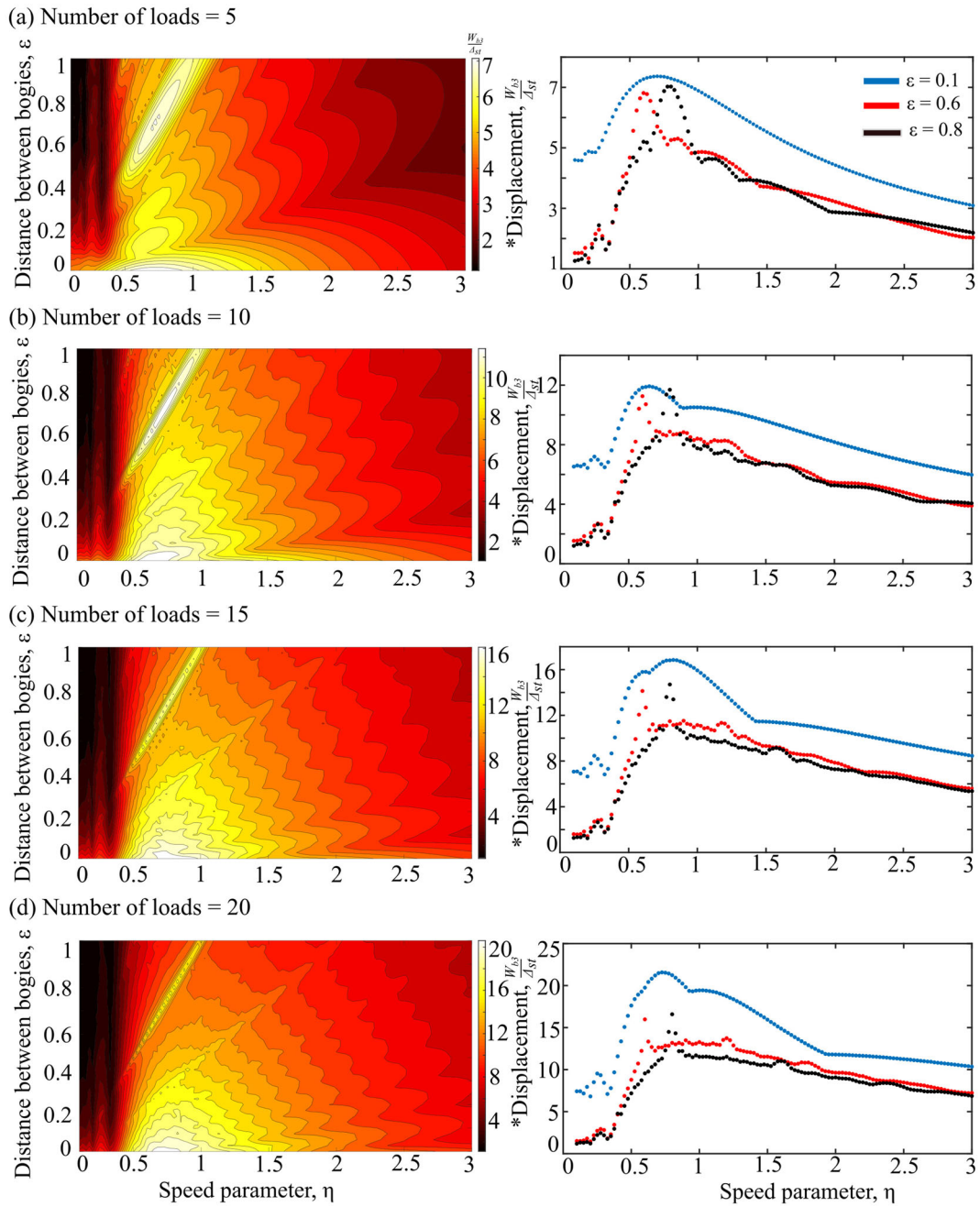
Figure 11. *Dimensionless displacement response for (a) number of loads = 5; (b) number of loads = 10; (c) number of loads = 15; and (d) number of loads = 20 for HSLM-B.
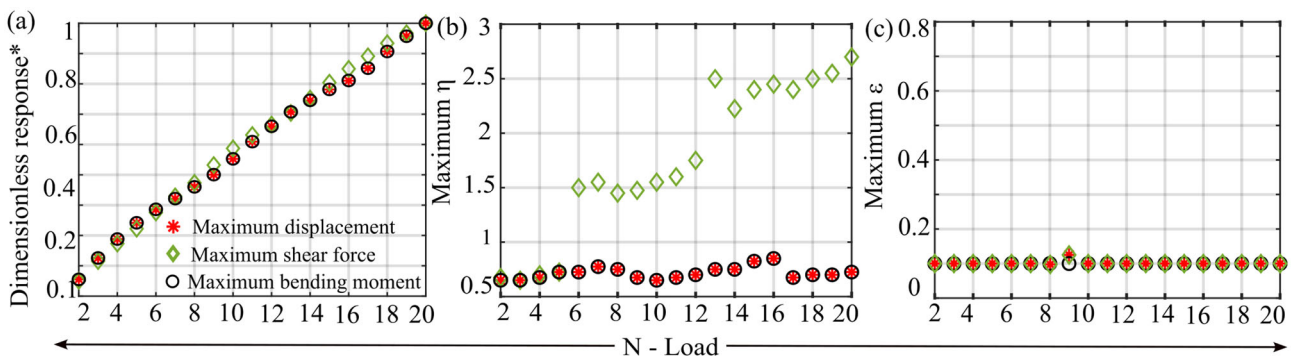
Figure 12. Variation of (a) *Normalised Dimensionless displacement response; (b) Maximum η; (c) Maximum ϵ for HSLM-B.
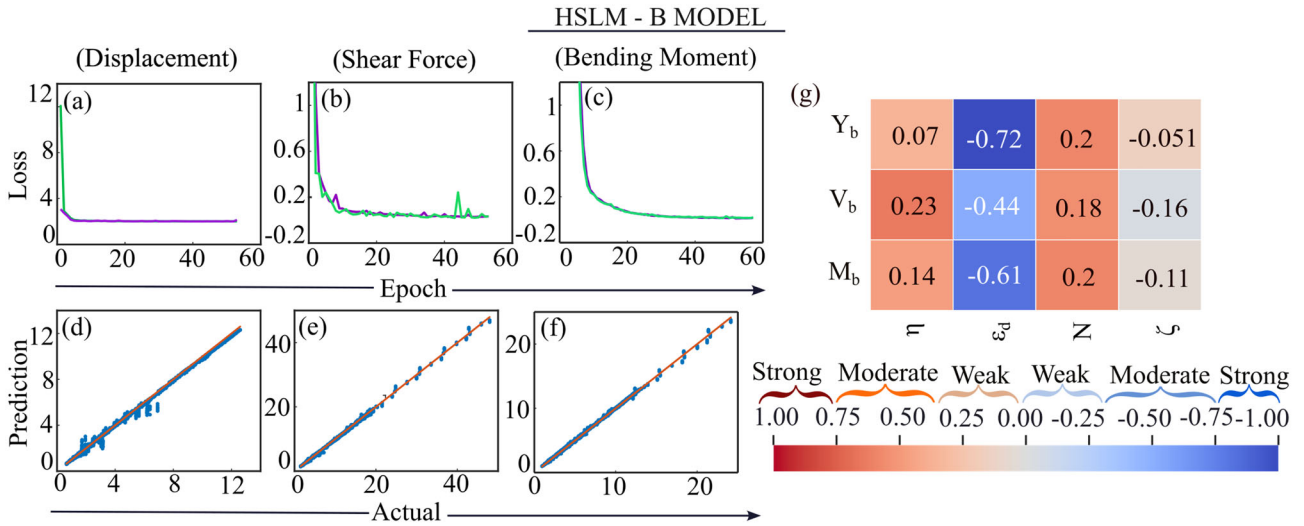
Figure 13. Loss versus epoch for (a) displacement; (b) shear force; (c) bending moment; Prediction versus actual for (d) displacement; (e) shear force; (f) bending moment; and (g) Pearson correlation matrix for HSLM-B with speed parameter η, distance between loads to the length of the bridge ϵ, number of loads N, and damping ζ.

Table 9. Metrices for the HSLM-B model.

	HSLM-B		
Output parameter	MSE	RMS	EVS
Displacement	0.0189	0.033	0.999
Shear force	0.0901	0.167	0.9989
Bending moment	0.06	0.116	0.998

Table 10. Comparison of analytical and the ML-based model for HSLM-B.

Speed (m/s)	29.52	88.57	243.53	457.5
η	0.1	0.3	0.825	1.55
ϵ	0.1	0.65	0.325	0.45
N	6	17	20	21
ζ	0	0.03	0.05	0.0125
Y_b (m)	0.00284	0.00077	0.00175	0.00139
Y_{bML} (m)	0.00285	0.00076	0.00174	0.00141
Error (%)	0.35	0.7	0.11	1.32
V_b (kN)	11.47	40.87	71.81	70.78
V_{bML} (kN)	11.46	39.8	72.76	70.85
Error (%)	0.12	2.62	1.33	0.105
M_b (kN.m)	74.109	188.76	385.4	377.3
M_{bML} (kN.m)	74.106	190.15	448.8	401.29
Error (%)	0.003	0.74	1.9	2.12

Table 11. Dimensionless normalised values for different values of ϵ_b.

ϵ_b	Displacement	Shear force	Bending moment
0.1	96	105.1	96
0.2	84.79	94.48	84.79
0.3	77.42	87.3	77.42
0.4	70.13	78.78	70.13

the prediction and actual values of the best-fitted models were compared as shown in Figure 13d–f, respectively. The models used for the fitting produce a satisfactory result for the output parameters considered in this study. A comparison between the analytical solution and the MIMO model has been evaluated. The actual and predicted values for four different combinations of the input parameters have been considered arbitrarily, and error percentages have been highlighted in Table 10, which is within 2%.

The sensitivity of various parameters listed in Table 10 on output is illustrated in Figure 13g. The displacement, shear force, and bending moment of the beam possess a weak positive correlation with the speed parameter, η. However, these responses are susceptible to the ϵ, i.e. the distance between loads to the length of the bridge. As the value of ϵ decreases, the displacement response of the beam amplifies because of the interference caused by the closely-spaced loads under the combination (i) as dictated in Table 10. Further, the number of loads, N on the bridge, correlates moderately with the abovementioned outputs in the analysis. As N increases, the output responses increase. These results bear sufficient generality with the proposed analytical model as shown in Figure 12. The damping factor of the beam has a weak relationship with the output parameters (Table 11).

4.4. HSLM-A

For long-span bridges ($L > 7$ m), Eurocode (Bsi, 2002) suggests the practice of HSLM-A in which the articulated train system can be considered as bogie consisting of four loads separated by a time lag of T_b and T_c as shown in Figure 14a.

maximum η for the maximum displacement and bending moment to occur lies between 0.5 and 0.65; however, for shear force, it lies between 1.3 and 2.7 depending on the number of loads as shown in Figure 12b. Therefore, a lower range of $\eta = 0.1$ to 0.45 and a higher range of $\eta = 0.7$–1.2 would be recommended for the safe design of simply-supported bridges against displacement. Similarly, based on the number of loads a range of η 1.8–3 is safe for N-loads = 2–12 whereas 0.5–2 for N-loads > 12. The values of ϵ where the maximum dynamic displacement, shear force, and bending moment occurs varies for ϵ ranging from 0.1 to 0.2 as shown in Figure 12c.

The training and validation of the HSLM-B model have been presented in the form of loss versus epoch as shown in Figure 13a–c for output parameters mentioned in Table 2. The best fit models are obtained for epochs varying from 40 to 60, and the factors evaluated from the analysis, such as MSE, RMS, and EVS, are mentioned in Table 9. Further,

Figure 14. Conventional train model as bogie system with time lag, $\epsilon_D = 0.1$, $\epsilon_d = 0.1$ for $\eta = 0.4$ as per HSLM-A (a)*Dimensionless displacement of 2 individual bogie; (b)*Dimensionless displacement of bogies in cumulative form.
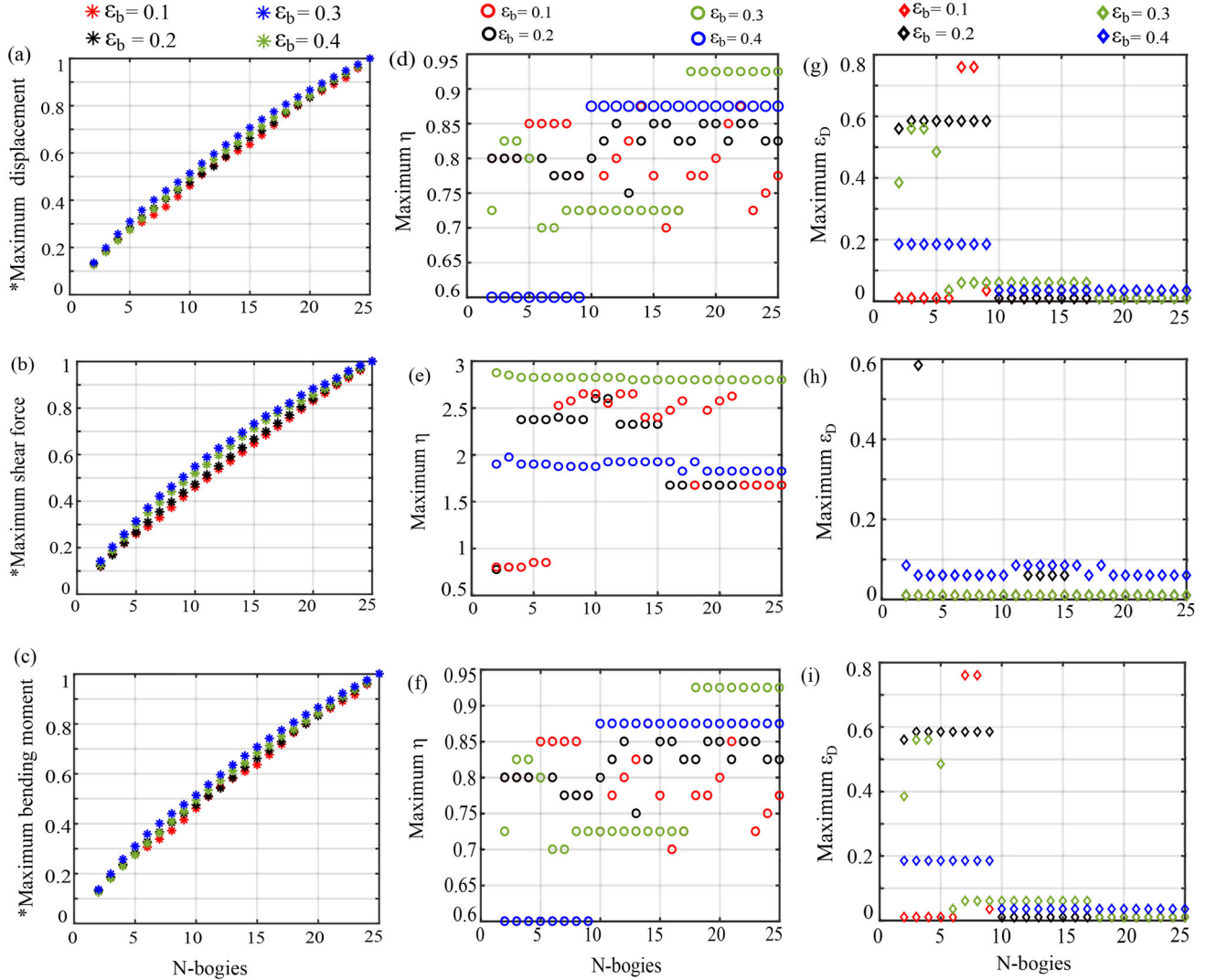
Figure 15. Variation of (a) *normalised dimensionless maximum displacement response; (b) *Normalised dimensionless maximum shear force response; (c) *normalised dimensionless maximum bending moment response; (d) maximum η corresponding to the *Normalised dimensionless maximum displacement response; (e) maximum η corresponding to the *Normalised dimensionless maximum displacement response; (f) maximum η corresponding to *Normalised dimensionless maximum shear force response; (g) maximum ϵ corresponding to *Normalised dimensionless maximum shear force response; (h) maximum ϵ corresponding to *Normalised dimensionless maximum bending moment response; (i) maximum ϵ corresponding to *Normalised dimensionless maximum bending moment response for HSLM-A.

The influencing parameters in this model can be regarded as:

- speed parameter, η,
- number of bogies (N-bogies),
- the ratio of the distance between wheels to the length of the bridge (b/L), ϵ_b, and

- the ratio of the distance between the first and last load in a bogie to the length of the bridge, ϵ_D.

The parameter ϵ_c can be expressed as the function of ϵ_b and ϵ_D as $\epsilon_D = 2\epsilon_b + \epsilon_c$, or $\epsilon_c = 1 - 2\epsilon_b$. Therefore, the values of ϵ_d should not exceed 0.5, and further analysis has been carried out for ϵ_b up to 0.4. Figure 15a,b shows the
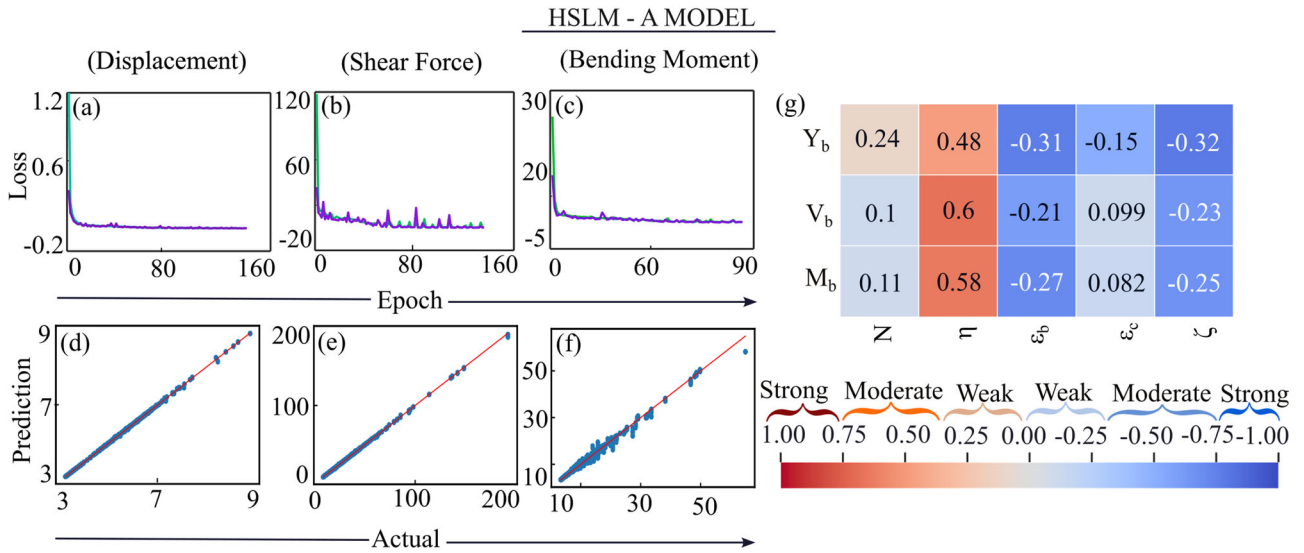
Figure 16. Loss versus epoch for (a) displacement; (b) shear force; (c) bending moment; Prediction versus actual for (d) displacement; (e) shear force; (f) Bending moment; and (g) Pearson correlation matrix for HSLM-A with the number of car units N-*bogies*, speed parameter η, the distance between loads to the length of the bridge ϵ_b, the distance between consecutive car units to the length of the bridge ϵ_c, and damping ζ.

Table 12. Metrices for the HSLM-A model.

	HSLM-A		
Output parameter	MSE	RMS	EVS
Displacement	0.0093	0.0155	0.9997
Shear force	0.172	0.3046	0.9997
Bending moment	0.2215	0.4812	0.9934

Table 13. Comparison of analytical and the ML-based model for HSLM-A.

Speed (m/s)	24.13	84.46	199.01	289.6
η	0.1	0.35	0.825	1.2
ϵ_d	0.1	0.3	0.6	0.2
ϵ_c	0.3	0.1	0.2	0.15
N	10	17	25	6
ζ	0.025	0.05	0.0425	0
$\bar{Y}_b$ (m)	0.00207	0.0022	0.0023	0.0028
$\bar{Y}_{b\,ML}$ (m)	0.00214	0.0024	0.00244	0.0029
Error (%)	3.7	5.57	5.42	3
$\bar{V}_b$ (kN)	1784.09	1565.45	2509.97	3547.2
$\bar{V}_{b\,ML}$ (kN)	1777.09	1539.22	2499.48	3585.68
Error (%)	0.39	1.67	0.42	0.105
M_b (kN m)	763.32	653.08	925.33	1484.87
$\bar{M}_{b\,ML}$ (kN m)	749.95	649.74	921.99	1469.85
Error (%)	1.75	0.51	0.36	1.01

dimensionless displacement response of individual two bogie system and their summation response, respectively. Figure 15 shows the maximum responses ((a) displacement, (b) shear force, and (c) bending moment) in dimensionless form normalised in a similar fashion as in HSLM-B, i.e. with respect to response values that occurred for 25 number of bogies presented in Table 11 for various values of ϵ_b. It can be noticed that the values are increasing with increasing bogies and the values of ϵ_b.

The maximum speed parameter at which maximum responses are attained can be obtained from Figure 15d–f. The maximum displacement and bending moment occur when η lies between 0.6 and 0.95, whereas the maximum shear force occurs when η is between 0.5 and 3 for different values of ϵ_b. The distance from centre to centre of bogies ϵ_D, which is responsible for much higher responses, lies

between 0.1 to 0.8 for displacement and bending moment; however, it is 0.1–0.6 for shear force, respectively. Based on the train configuration (number of bogies and their adjacent distances), one can safely design long-span simply supported bridges for the desired speed.

Similar to the single load model and HSLM-B, the loss versus epoch plots for training and validation loss were investigated as shown in Figure 16a–c. An epoch of 40-90 is sufficient to train the training losses with the validation loss. Further, the prediction and actual values of the fitted model were compared as shown in Figure 16d–f. The statistical evaluation for the fitted models for HSLM-A is noted in Table 12. A case study with different combinations of input parameters has been considered the study for a constant value of the distance between the rear and far wheels in a car unit, $D = 1$. It can be observed that the difference in the actual and predicted values varies within 6% for the output parameters as shown in Table 13, which is within the acceptable limits of accuracy.

In the case of HSLM-A, the number of car units N has a weak positive correlation with all the output parameters. The speed parameter has a moderate to strong positive correlation with displacement, shear force, and bending moment. Further, the distance between loads ϵ_b has more sensitivity on output than the distance between the consecutive car units ϵ_c. Additionally, the damping of the bridge possesses a weak relationship with the output parameters.

5. Interface

A user-defined interface has been provided with three modules for three different load models; one of them (HSLM-B) has been shown in Figure 17. The steps to be followed by the respective user is described as follows:

- The details of moving load such as wheel load, number of loads, the distance between the rear and front wheels,

User-defined Interface

Figure 17. User-defined interface for the design of simply-supported bridges under high-speed train loads.

and consecutive distance between car units have to be provided. Similarly, the bridge parameters such as length, flexural rigidity, mass per unit length, etc., have to be filled in the initial step.

- For short-span bridges (L < 7 m), HSLM-B is recommended, and for bridges span > 7m, HSLM-A is recommended by codal provision.
- By clicking the compute button, the respective responses, such as displacement, shear force, and bending moment, can be assessed.
- Further, the obtained displacement response of the bridge deck can be checked against the values provided in the Eurocode EN 1990:2002 + A1:2005 (E), clause A2.4.4.2.3 according to which the maximum vertical displacement should not exceed L/600.
- A Disclaimer at the end will represent whether the permitted bridge displacement is safe or unsafe.

The details of the publicly available user-defined dashboard have been provided https://github.com/SusmitaIITDmetalab/Susmita_Meta.git upon the publication of the work.

6. Conclusions

The present study illustrates the combined multi-modal response combining forced and free vibration of a simply supported beam subjected to different models of moving loads in dimensionless form. Further, the accuracy of the model has been verified with the available literature. Finally, an artificial neural network-based multi-input multi-output metamodel is developed for predicting the design parameters bypassing all these extensive semi-analytical computations. The development of the semi-analytical framework for the prediction of peak dynamic responses of the bridge in conjunction with ANN-based MIMO metamodeling is the prime novelty of the article. The important conclusions that can be drawn are as follows:

- With the variation of the speed parameter η, the dynamic displacement increases and reaches the maximum at $\eta = 0.6$–0.65 and thereafter decreases for the moving load models considered in this study, namely single load model, HSLM-B and HSLM-A, respectively.
- Forced vibration dominates for $\eta < 1$, while for $\eta > 1$ the accumulation of free vibration influences the dynamic response of the bridge.
- The position of maximum displacement occurs at mid-span; however, the location of maximum bending moment is dependent on the mode under consideration as well as the speed parameter. The location of the maximum amplitude of shear force always occurs at either end of the beam.
- The dynamic responses of the defined load models possess strong to moderate correlation with speed parameters η and ϵ, i.e. the distance between wheel loads to the length of the bridge.
- In the case of HSLM-B, the maximum displacement response is attained at $\eta = 0.5$ to 0.65. However, for shear force and bending moment, the values of η vary from 2.5 to 3, and ϵ varies from 0.1 to 0.2.
- With the increase in values of ϵ_b in the HSLM-A model, the dynamic responses (displacement, shear force, and bending moment) increase. The maximum dynamic displacement and bending moment occur for $\epsilon_D = 0.1$ to 0.8 for a range of $\eta = 0.6$ to 0.95. However, maximum shear force occurs for range of $\epsilon_D = 0.1$ to 0.6 for $\eta = 0.5$ to 3 for different configuration values of ϵ_b.

- A maximum error of 1%, 2%, and 6% is noticed in the prediction of the design parameters using ANN-based metamodel with that of the semi-analytical model for single load, HSLM-B, and HSLM-A.

The effect of factors such as rail irregularities and fatigue has not been included in the present scope of work and can be considered as the limitation of the proposed theory. Further, the cumbersome process of complicated analytical formulations can be reduced with a cost-efficiency cognitive structure of ANN-based metamodels. Such MIMO models possess huge future applications in high-speed bridge designing and optimising the design parameters for vibration control of bridges.

Acknowledgements

Disclosure statement

No potential conflict of interest was reported by the authors.

References

Arvidsson, T., & Karoumi, R. (2014). Train–bridge interaction–a review and discussion of key model parameters. *International Journal of Rail Transportation*, 2(3), 147–186. ISSN 2324–8386.

Benesty, J., Chen, J., Huang, Y., & Cohen, I. (2009). Pearson correlation coefficient. In *Noise reduction in speech processing* (pp. 1–4). Berlin, Heidelberg: Springer-Verlag.

Bsi, B. (2002). *Eurocode: Basis of structural design* (p. 114). London: British Standards Institute.

Cantero, D., Arvidsson, T., OBrien, E., & Karoumi, R. (2016). Train–track–bridge modelling and review of parameters. *Structure and Infrastructure Engineering*, 12(9), 1051–1064.

Edwards, A. L. (1976). An introduction to linear regression and correlation. *The Correlation Coefficient*, pages, 33–46.

Fang, C., Tang, H., Li, Y., & Wang, Z. (2020). Effects of random winds and waves on a long-span cross-sea bridge using bayesian regularized back propagation neural network. *Advances in Structural Engineering*, 23(4), 733–748.

Garmendia, M., Ribalaygua, C., & Ureña, J. M. (2012). High speed rail: implication for cities. *Cities*, 29, S26–S31.

Gbadeyan, J., & Oni, S. (1995). Dynamic behaviour of beams and rectangular plates under moving loads. *Journal of Sound and Vibration*, 182(5), 677–695.

Glen, S. (2021). Correlation coefficient: Simple definition, formula, easy steps. Statistics How To.com. https://www. statisticshowto. com/probability-and-statistics/correlation-coefficient-formula/

Goldberg, D. E. (2013). *Genetic algorithms*. Pearson Education , Dorling Kindersley (India) Pvt. Ltd.

Gordan, M., Sabbagh-Yazdi, S.-R., Ismail, Z., Ghaedi, K., Carroll, P., McCrum, D., & Samali, B. (2022). State-of-the-art review on advancements of data mining in structural health monitoring. *Measurement*, 193, 110939.

Grandi, J., & Ramondenc, P. (1990). *The dynamic behavior of railways on high speed lines*. SNCF.

Han, X., Xiang, H., Li, Y., & Wang, Y. (2019). Predictions of vertical train-bridge response using artificial neural network-based surrogate model. *Advances in Structural Engineering*, 22(12), 2712–2723.

Han, Z.-H., & Zhang, K.-S., et al. (2012). Surrogate-based optimization. *Real-World Applications of Genetic Algorithms*, 343–362.

Huang, Y., & Fu, J. (2019). Review on application of artificial intelligence in civil engineering. *Computer Modeling in Engineering & Sciences*, 121(3), 845–875.

Jin, S., & Feng, H. D. (2020). Reliability assessment of a curved heavy-haul railway track-bridge system. *Structure and Infrastructure Engineering*, 16(3), 465–480.

Kang, C., Schneider, S., Wenner, M., & Marx, S. (2018). Development of design and construction of high-speed railway bridges in Germany. *Engineering Structures*, 163, 184–196.

Kaynia, A. M., Madshus, C., & Zackrisson, P. (2000). Ground vibration from high-speed trains: prediction and countermeasure. *Journal of Geotechnical and Geoenvironmental Engineering*, 126(6), 531–537.

Kullaa, J. (2009). Eliminating environmental or operational influences in structural health monitoring using the missing data analysis. *Journal of Intelligent Material Systems and Structures*, 20(11), 1381–1390.

Li, Y.-T., & Schmöcker, J.-D. (2017). Adaptation patterns to high speed rail usage in Taiwan and China. *Transportation*, 44(4), 807–830.

Li, H., Wang, T., & Wu, G. (2021). Dynamic response prediction of vehicle-bridge interaction system using feedforward neural network and deep long short-term memory network. *Structures* (Vol. 34, pp. 2415–2431). Elsevier.

Li, H., Wang, T., & Wu, G. (2021b). Probabilistic safety analysis of coupled train-bridge system using deep learning based surrogate model. *Structure and Infrastructure Engineering*, 1–20.

Li, H., Wang, T., & Wu, G. (2022). A bayesian deep learning approach for random vibration analysis of bridges subjected to vehicle dynamic interaction. *Mechanical Systems and Signal Processing*, 170, 108799.

Lu, P., Chen, S., & Zheng, Y. (2012). Artificial intelligence in civil engineering. *Mathematical Problems in Engineering*, 2012

Mete, F., Chen, Y., Stathopoulos, A., & Corr, D. J. (2019). Comparative study of predictive analysis methods to estimate bridge response. *Transportation Research Record*, 2673(9), 365–376.

Modarres, C., Astorga, N., Droguett, E. L., & Meruane, V. (2018). Convolutional neural networks for automated damage recognition and damage type identification. *Structural Control and Health Monitoring*, 25(10), e2230.

Museros, P., & Alarcón, E. (2002). An investigation on the importance of train-bridge interaction at resonance. In *Proceedings of the sixth conference on Computational structures technology* (pp. 335–336).

Ok, S., Son, W., & Lim, Y. (2012). A study of the use of artificial neural networks to estimate dynamic displacements due to dynamic loads in bridges. In *Journal of Physics: Conference Series*, Modern Practice in Stress and Vibration Analysis 2012 (MPSVA 2012) , University of Glasgow, (Vol. 382, p. 12032). IOP Publishing.

Olsson, M. (1991). On the fundamental moving load problem. *Journal of Sound and Vibration*, 145(2), 299–307.

Rocha, J. M., Henriques, A. A., & Calçada, R. (2016). Probabilistic assessment of the train running safety on a short-span high-speed railway bridge. *Structure and Infrastructure Engineering*, 12(1), 78–92.

Salcher, P., Adam, C., & Kuisle, A. (2019). A stochastic view on the effect of random rail irregularities on railway bridge vibrations. *Structure and Infrastructure Engineering*, 15(12), 1649–1664.

Salehi, H., & Burgueño, R. (2018). Emerging artificial intelligence methods in structural engineering. *Engineering Structures*, 171, 170–189.

Sedgwick, P. (2012). Pearson's correlation coefficient. *BMJ*, 345, e4483.

Sugawara, M. (1995). Urban transportation in Asian countries. *Japan Railway and Transport Review*, 4, 23–34.

Sun, L., Shang, Z., Xia, Y., Bhowmick, S., & Nagarajaiah, S. (2020). Review of bridge structural health monitoring aided by big data and artificial intelligence: From condition assessment to damage detection. *Journal of Structural Engineering*, 146(5), 4020073.

Suryanita, R., & Adnan, A. (2013). Application of neural networks in bridge health prediction based on acceleration and displacement data domain. In *Proceedings of the International MultiConference of Engineers and Computer Scientists* (vol. 1 pp. 13–15).

Suryanita, R., & Adnan, A. (2014). Early-warning system in bridge monitoring based on acceleration and displacement data domain, In: Yang, GC., Ao, SI., Huang, X., Castillo, O. (Eds.), *Transactions*

on Engineering Technologies (Vol. 275, pp. 157–169). Lecture Notes in Electrical Engineering, Springer, Dordrecht.

Tang, Q., Xin, J., Jiang, Y., Zhou, J., Li, S., & Chen, Z. (2022). Novel identification technique of moving loads using the random response power spectral density and deep transfer learning. *Measurement*, *195*, 111120.

Thai, H.-T. (2022). Machine learning for structural engineering: A state-of-the-art review. *Structures* (Vol. 38, pp. 448–491).

Vodithala, S., Mahendar, A., & Bhuya, S. (2020). Damage prediction techniques for structural health monitoring in bridge using sensors and ann-machine learning technique. *International Journal of Future Generation Communication and Networking*, *13*(4), 3222–3231.

Wang, C., Duan, Q., Gong, W., Ye, A., Di, Z., & Miao, C. (2014). An evaluation of adaptive surrogate modeling based optimization with two benchmark problems. *Environmental Modelling & Software*, *60*, 167–179.

Wedel, F., & Marx, S. (2022). Application of machine learning methods on real bridge monitoring data. *Engineering Structures*, *250*, 113365.

Xia, H., & Zhang, N. (2005). Dynamic analysis of railway bridge under high-speed trains. *Computers & Structures*, *83*(23-24), 1891–1901.

Xu, J. (2020). Machine learning-based dynamic response prediction of high-speed railway bridges.

Yang, Y.-B., Yau, J.-D., & Hsu, L.-C. (1997). Vibration of simple beams due to trains moving at high speeds. *Engineering Structures*, *19*(11), 936–944.

Yang, Y.-B., Yau, J., Yao, Z., & Wu, Y. (2004). *Vehicle-bridge interaction dynamics: with applications to high-speed railways*. World Scientific Publishing Company

Yau, J.-D., Yang, Y.-B., & Kuo, S.-R. (1999). Impact response of high speed rail bridges and riding comfort of rail cars. *Engineering Structures*, *21*(9), 836–844.

Yu, Y., Cai, C., & Deng, L. (2016). State-of-the-art review on bridge weigh-in-motion technology. *Advances in Structural Engineering*, *19*(9), 1514–1530.

Appendix

Notation

ρA	mass per unit area
EI	flexural rigidity
C_b	damping coefficient of the bridge
P_V	forces due to the moving load
$\tilde{W}_b$	dynamic displacement of the bridge
x	position on the bridge
t	time taken by moving force to travel the bridge
$\delta(x)$	dirac-delta function
v	speed of the moving vehicle
L	length of bridge
d	axle spacing
d/v	time lag
P_0	gravitational weight of the running train
$P(t)$	step function
t_{kd}	time delay of kth load in HSLM-B model
t_{kD}	time delay of kth load in HSLM-A model
$Q_{bj}(t)$	generalised coordinate
$\phi_j(x)$	shape function of jth mode
$\tilde{V}$	shear force
$\tilde{M}$	bending moment
M	dimensionless bending moment
V	dimensionless shear force
ω	frequency of vibration of moving load
ω_{bj}	natural frequency of the beam for $jth^$ mode
ω_b	natural frequency of the beam for first mode
ζ_b	damping coefficient
C_c	critical damping constant
$Q_{bj}(x,t)$	dimensionless displacement of beam
Δ_{st}	static constant
a	dimensionless length over the bridge
τ	dimensionless time
$\bar{\tau}$	dimensionless time for HSLM-B
η	speed parameter
N-bogies	number of bogies
ϵ_d	ratio of the distance between loads to the length of the bridge in HSLM-B model
ϵ_D	ratio of the distance of a single bogie to the length of the bridge
ω_d	damped frequency of vibration of the beam
$M_v, C_v, K_v,$ and F_v	mass, damping, stiffness, and force matrices
t_{kD} and $\bar{\tau}_D$	time taken and corresponding time lag of the $kth^$ bogie separated by ϵ_D
t_b and $\bar{\tau}_b$	time taken and corresponding time lag of loads P_{t1} and P_{t2} separated by ϵ_d
t_c and $\bar{\tau}_c$	time taken and corresponding time lag of loads P_{t1} and P_{t3} separated by ϵ_c